ENTANGLED PHOTONS REGENERATION USING FIBER RING RESONATOR INCORPORATING AN ERBIUM-DOPED FIBER

WANCHAI KHUNNAM

A THESIS SUBMITTED IN PARTIAL FULFILLMENT

OF THE REQUIREMENT FOR THE DEGREE OF

DOCTOR OF PHILOSOPHY IN APPLIED PHYSICS

SCHOOL OF GRADUATE STUDIES

KING MONGKUT'S INSTITUTE OF TECHNOLOGY LADKRABANG

2008

KMITL-2008-SC-D-030-428

หัวข้อวิทยานิพนธ์	การสร้างโฟตอนเกี่ยวพันกันขึ้นใหม่ โดยใช้โพรงสั่นพ้องวงแหวนร่วมกับเส้นใยนำแสงเออร์เบียมโดป
นักศึกษา	นายวันชัย ขันนาม
รหัสประจำตัว	47063453
ปริญญา	ปรัชญาดุษฎีบัณฑิต
สาขาวิชา	ฟิสิกส์ประยุกต์
พ.ศ.	2551
อาจารย์ผู้ควบคุมวิทยานิพนธ์	รศ.ดร. ปรีชา ยุพาพิน

บทคัดย่อ

งานวิจัยนี้เป็นการนำเสนอการศึกษาการสร้างโฟตอนเกี่ยวพันกันขึ้นใหม่ โดยใช้โพรงสั่นพ้องวงแหวนร่วมกับเส้นใยนำแสงเออร์เบียมโดป เมื่อสถานะโฟตอนเกี่ยวพันกันที่มีความเข้มแสงต่ำวิ่งผ่านโพรงสั่นพ้องวงแหวนร่วมกับเส้นใยนำแสงเออร์เบียมโดป โดยเส้นใยนำแสงเออร์เบียมโดปเป็นตัวกลางที่สามารถขยายสัญญาณแสง สัญญาณเอาท์พุตของสถานะโฟตอนเกี่ยวพันกันก็จะถูกสร้างขึ้นใหม่ โดยมีตัวควบคุมสถานะโพลาไรซ์ ระหว่างที่แสงวิ่งในโพรงสั่นพ้องวงแหวนซึ่งจะมีการเพิ่มจำนวนโฟตอนที่ถูกควบคุมสถานะโพลาไรซ์เกิดขึ้น ทำให้เกิดการซ้อนทับของความไม่เป็นเชิงเส้นทางแสงแบบสุ่ม เกิดโฟร์เว็ฟมิกซ์ซิ่ง ผลการศึกษาแสดงให้เห็นว่าเราสามารถสร้างสถานะโพลาไรซ์โฟตอนเกี่ยวพันกันได้ โดยการขยายสัญญาณแสงทำให้สถานะโฟตอนมีความเข้มแสงสูงขึ้น ผลที่ได้ทำให้โฟตอนเกี่ยวพันกันมีสถานะที่ชัดเจนมากขึ้น และทำการทดลองผลกระทบของอุณหภูมิต่อสถานะโฟตอนเกี่ยวพันกัน อุณหภูมิทำให้เฟสของโฟตอนเปลี่ยนไป หมายความว่าสถานะโฟตอนเกี่ยวพันกันเกิดการวอล์กออฟ เมื่อมีการเปลี่ยนแปลงอุณหภูมิเปลี่ยน เราสามารถชดเชยด้วยการใช้ตัวควบคุมสถานะโพลาไรซ์

Thesis Title	Entangled Photons Regeneration using Fiber Ring Resonator Incorporating an Erbium-doped Fiber.
Student	Mr. Wanchai Khunnam
Student ID	47063453
Degree	Doctor of Philosophy
Program	Applied Physics
Year	2008
Thesis Advisor	Assoc. Prof. Dr. Preecha Yupapin

ABSTRACT

In this thesis present a study of the entangled photons states regeneration by using a fiber ring resonator incorporating an erbium-doped fiber (EDF) has been investigated. We have shown that the weak entangled photons states can be recovered after circulating in the amplified fiber optic medium. The output entangled photons states can be re-generated by adjusting the polarization controller of the amplified photons. where the re-generated entangled states can be controlled and performed. A polarization controller controls polarization states of light pulses while they circulate in the ring resonator. The superposition of the nonlinear light pulses in a fiber optic ring resonator randomly occur by nonlinear four-wave mixing type. The results obtained have shown that this system can be used to achieve the recovered polarization entangled states with the obtained high gain. The amplifying noise has also been detected and seen on the spectrum output. This is affected to the entangled photons visibility. An investigation the thermal effects on the entangled photons states. The relationship between thermal effects and the entangled states phase shift. Which means the entangled photons states walk-off due to the change in temperature could be compensated and achieved by using a pair of the polarization control devices. This is shown that the changes in phase of the entangled photons can be negligible when the compensation is employed.

ACKNOWLEDGEMENTS

First of all, I would like to thank Assoc. Prof. Dr. Preecha Yupapin, my advisors head of Advanced Research Center for Photonic Laboratory(ARCP) King Mongkut Institute of Technology Ladkrabang (KMITL) for granting me the opportunity to work on the topic of this dissertation. During my work at ARCP Laboratory, his provided me any support possible and has always been open for discussions and problems, both during the time of the experiments and during the writing of the thesis. I would like to thank Assist. Prof. Dr. Surasak Chiangga for helping in give me advice to approve my thesis.

I would like to thank my co-workers at the Advanced Research Center for Photonic Laboratory have been to this work, particularly S. Suchat, P. Saeung, P. Chanpang, W. Suwancharoen, C. Sripakdee, A.Sangthong, S.Thongmee and S. Chaiyatsoonthorn. Thanks are also to Mahanakhon University of Technology (MUT) for support some device and instrument of my research. Thank a lot for my friends at Department of Applied Physics Faculty of Science KMITL, for friendly and good thinks for me.

Finally, I wish to thank Department of Physics, Faculty of Science, Nareasuan University, Pitsanulok. Province Thailand for financial support of my study. And most importantly, I owe a debt of gratitude to my family and my wife Mrs.Kanchana for all their love and support all my life.

WANCHAI KHUNNAM

CONTENTS

Pages

CONTENTS (Cont.)

CONTENTS (Cont.)

LIST OF FIGURES

Figures **Pages**

LIST OF FIGURES (Cont.)

Figures **Pages**

CHAPTER 1

INTRODUCTION

1.1 Motivation

Quantum communication has become the popular system of the communication link, because its advantage utilizes the information security. The required information can be secured by using a technique known as quantum cryptography. Up to now, there are several systems that can be performed the quantum cryptography via communication link. The free space link has been proposed by Manderbach et al. [1]. Recently, the use of quantum cryptography via satellite has also been proposed by Pfennigbauer et al. [2]. They have shown the very promising results of the key requirement i.e. information security, where the implementation of the quantum cryptography in the communication network is plausible. However, the basic problem of the long distance link is occurred by the common effect i.e. signal degradation, therefore, the technique of signal amplification will be the subject of the investigation, especially, the signal recovery. Recently, Suchat and Yupapin [3] proposes a new system of quantum key distribution via an optical wireless communication links, where the required information is secured by using a quantum code/decode (CODEC) technique incorporating in the networks. The proposed system consists of a quantum key, uplink and downlink parts that can be implemented in the mobile telephone hand set and networks. The idea of the quantum repeater has been proposed for long-distance entanglement [4]. This is created by distributing the entangled states over sufficiently short segments of a channel, which can be purified and connected via the entanglement. However, due to their rather low success probabilities in the initial entanglement distribution, these protocols feature the very low communication rates. In case of the system using weak light input (i.e. without pumping part and component), the fiber acts as a nonlinear medium because of the optical Kerr effect and four-wave mixing in fiber ring resonator. When a polarized pulse or polarization entangled photons enters into a fiber ring resonator incorporating an erbium-doped fiber (EDF) , the nonlinear effect i.e. Kerr type occurs which is induced the entangled states as [5]. Recentry,Yupapin et al. [6] have reported a very promising technique of signal transmission security using chaotic behaviors of light propagating in a nonlinear fiber ring resonator. The required signal can be secured by using the chaotic signal waveform , where the signal retrieval can be introduced by the end users. Using this technique ,the chaotic codes can be also generated , which has been proposed by Yupapin and Suwancharoen [7],

The major parameters of the system which can be induced the chaotic behavavior of light while traveling within the fiber ring resonator are a fiber ring radius and input optical power.

Quantum entanglement is a physical resource, like energy, associated with the peculiar nonclassical correlations that are possible between separated quantum systems. In effect, the very possibility of considering a particle or system as possessing objective properties depends on its entanglement with another particle or system. Quantum entanglement has been widely studied and investigated during the 1990s. The Austrian-born Erwin Schrodinger, who in 1933 shared the Nobel Prize with Paul Dirac, introduced the conventional idea. Albert Einstein proposed a situation that came to known as the EPR (Einstein-Podolsky-Rosen) paradox, where he called attention to the fact that while it was impossible to know whether a single photon would pass or be absorbed by a filter paired photons. Would a subject to the same polarization test always being entangled. The experiment simply succeeded, where the entangled went of a single/two photons was observed and this has been used in some applications in quantum cloning, quantum teleportation, measurement and cryptography.

1.2 Objective of the Study

1.2.1 Study process of entangled photons generation using fiber optic.

1.2.2 Study the ring resonator incorporating erbium-doped fiber

1.2.3 Study the entangled photons states regeneration.

1.2.4 Study the entangled photons state walk-off compensation.

1.3 Scope of Study

The aim of this study is to show that the entangled photons regeneration study based on fiber optic ring resonator, and then we will show properties of the experiment methods. We will then make a conclusion the properties of each method.

1.4 Process of the Study

1.4.1 Study the theory of fiber optic ring resonator.

1.4.2 Study the theory of quantum entangled photons generation.

1.4.3 Study the theory of the erbium-doped fiber amplifier.

1.4.4 Set up on the entangled photons regeneration system using fiber optic ring resonator incorporating erbium-doped fiber optic.

1.4.5 Conclude and discuss the results.

1.5 Expected Results

1.5.1 Important physical meaning; i.e of quantum and entangled photons sates regeneration will be clearly understood.

1.5.2 Effects of temperature, nonlinear effect in fiber ring resonator, and external applied will be acknowledged.

1.5.3 Potential advantages of fiber optic ring resonator and entangled photons generation are utilized.

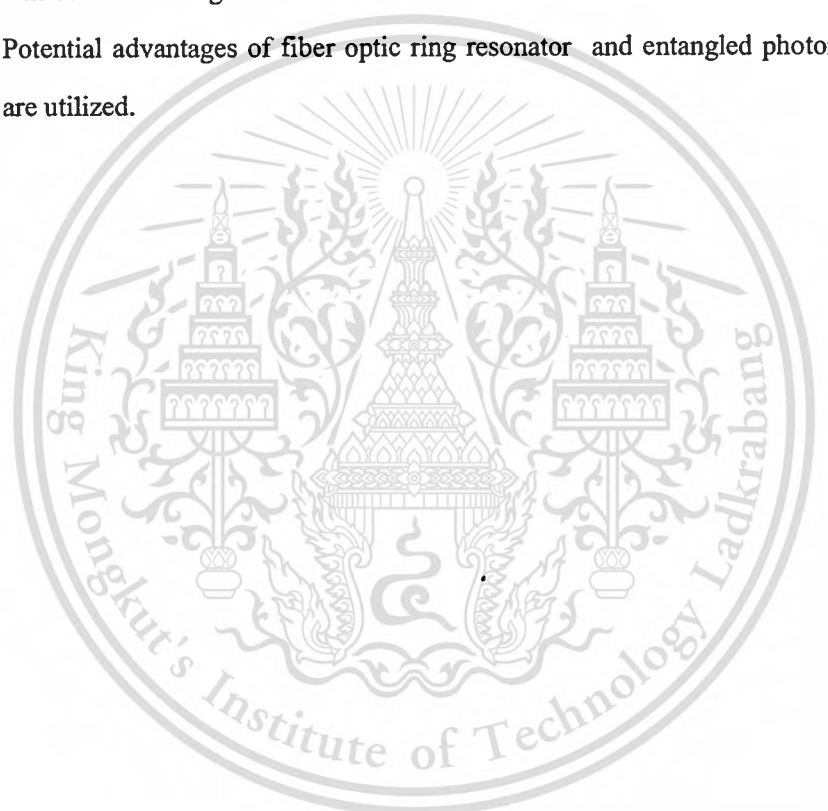

CHAPTER 2

RING RESONATOR

In this chapter, I will describe the material system which was used for the planar waveguide and the theoretical of ring resonator, resonance characteristics of ring resonators, fiber optic ring resonator and processes that affect the performance of material system which was used for fiber optic.

2.1 The Ring Resonator

The proposal to use an integrated ring resonator for a band pass filter has been made in 1969 by E. A. Marcatili. The transmission properties of the used guide consisting of a dielectric rod with rectangular cross section, surrounded by several dielectrics of smaller refractive indices have been described by E. A. Marcatili .A general architecture for an autoregressive planar waveguide optical filter was demonstrated for the first time in 1996. The autoregressive lattice filters which were designed and fabricated consisted of one and two stages using Ge-doped silica waveguides.

A signal flow chart transformation for evaluating the filter transfer functions was demonstrated. Purely passive single ring resonator filters have been realized in the material system AlGaAs-GaAs and Si-SiO_2 and Si_3N_4- SiO_2. The radius of the used ring resonators is between 5 μm and 30 μm and the free spectral range (FSR) achieved is between 20 nm and 30 nm. Passive ring resonators in the form of a racetrack have been realized in the material system GaInAsP and AlGaAs-GaAs. The filter performance is limited by bending and scattering losses in the resonator. These losses could be compensated for by using an active material instead or in addition.

2.2 Basic Ring Resonator

A ring resonator is simply a waveguide shaped into a ring structure as shown in Fig. 2.1 When an input electric field, E_i is coupled to the ring waveguide through an external bus waveguide, a positive feedback is induced and the field inside the ring resonator, E_{r2} starts to build up. Coupling between the straight and the ring waveguide is achieved through the evanescent wave. Therefore, the gap and coupling length between them determine how much

power is coupled from the straight waveguide to the ring waveguide and vise versa. The feedback mechanism is simply induced by the ring waveguide and therefore there is no need for any Bragg gratings, mirrors, or distributed feedback waveguides which are more difficult to fabricate. In such configuration, only certain wavelengths will be allowed to resonate inside the ring waveguide, thus frequency selectivity is obtained.

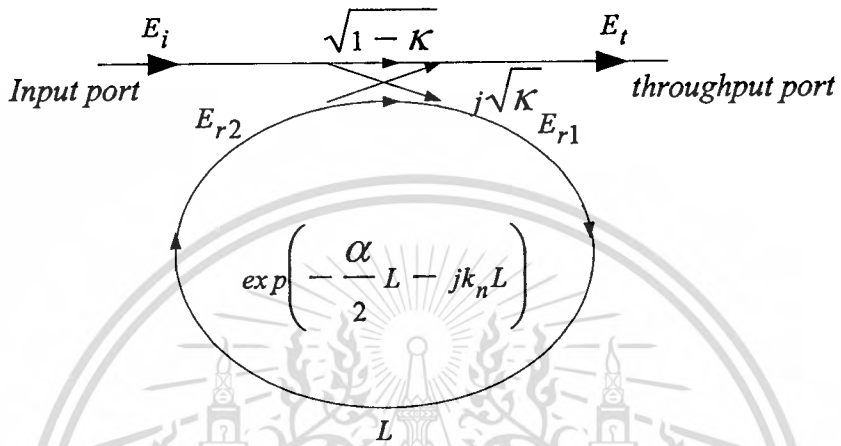

Fig. 2.1 Schematic diagram for a ring resonator coupled to a single waveguide.

The transfer function of this configuration is derived using Z-transform analysis. The circumference of the ring is L ($L = 2\pi R$, the radius is R), the coupling coefficient of the coupler is κ. The Z-transform parameter is represented by $z^{-1} = \exp^{-jk_nL}$ where $k_n = \frac{2\pi}{\lambda} n_{eff}$ is the propagation constant and n_{eff} is the effective index of the waveguide. The one round trip loss is $a = \exp^{-\alpha L/2}$, α is the intensity attenuation coefficient inside the waveguide [unit $length^{-1}$]. The transmitted or throughput field at the output of the straight waveguide, E_t and inserted electric field, E_i relations can be derived as followed:

$$E_t = (1-\gamma)^{1/2} \times \left[E_i \cdot \sqrt{1-\kappa} + j \cdot E_{r2}\sqrt{\kappa}\right]. \quad (2.1)$$

$$E_{r1} = (1-\gamma)^{1/2} \times \left[j \cdot E_i \cdot \sqrt{\kappa} + E_{r2} \cdot \sqrt{1-\kappa}\right]. \quad (2.2)$$

$$E_{r2} = E_{r1} \cdot a\, z^{-1}. \quad (2.3)$$

Using these equations, E_t / E_i can be calculated:

$$\frac{E_t}{E_i} = (1-\gamma)^{1/2} \times \left[\frac{\sqrt{1-\kappa} - (1-\gamma)^{1/2} \cdot a z^{-1}}{1 - (1-\gamma)^{1/2} \cdot \sqrt{1-\kappa} \cdot a z^{-1}} \right]. \tag{2.4}$$

The transfer function in Eq. (2.4) indicates that a ring resonator is very similar to a Fabry-Perot cavity. In the particular case shown in Fig. 2.1, the corresponding Fabry-Perot cavity would have an input mirror with a field reflectivity and a fully reflecting output mirror. However, the field propagating inside the ring cavity is a traveling wave in contrast to the Fabry-Perot cavity which resonates a standing wave.

In the following, new parameter will be used for simplification:

$$\begin{aligned} D &= (1-\gamma)^{1/2} \\ x &= D \cdot \exp^{-\alpha L/2} \\ y &= \sqrt{1-\kappa} \\ \phi &= k_n \cdot L \end{aligned} \tag{2.5}$$

The intensity relation for the output port is given by:

$$T = \frac{I_t}{I_i}(\phi) = \left| \frac{E_t}{E_i} \right|^2 = D^2 \cdot \left[1 - \frac{(1-x^2)\cdot(1-y^2)}{(1-x\cdot y)^2 + 4\cdot x\cdot y\cdot \sin^2\left(\frac{\phi}{2}\right)} \right]. \tag{2.6}$$

The transmission spectrum of a single ring resonator is shown in Fig. 2.2. The maximum and minimum transmission is calculated, using:

$$T_{\max} = D^2 \cdot \frac{(x+y)^2}{(1+x\cdot y)^2}. \tag{2.7}$$

$$T_{\min} = D^2 \cdot \frac{(x-y)^2}{(1-x\cdot y)^2}. \tag{2.8}$$

The minimum transmission $T_{\min}$, occurs at resonant point when the circumference of the ring L, is an integral number of guide wavelength which is defined by

$$\phi = k_n \cdot L = 2m\pi, \qquad m = integer$$
$$m \cdot \lambda_m = n \cdot L. \tag{2.9}$$

Here, m is the mode number, λ_m is the resonant mode wavelength.

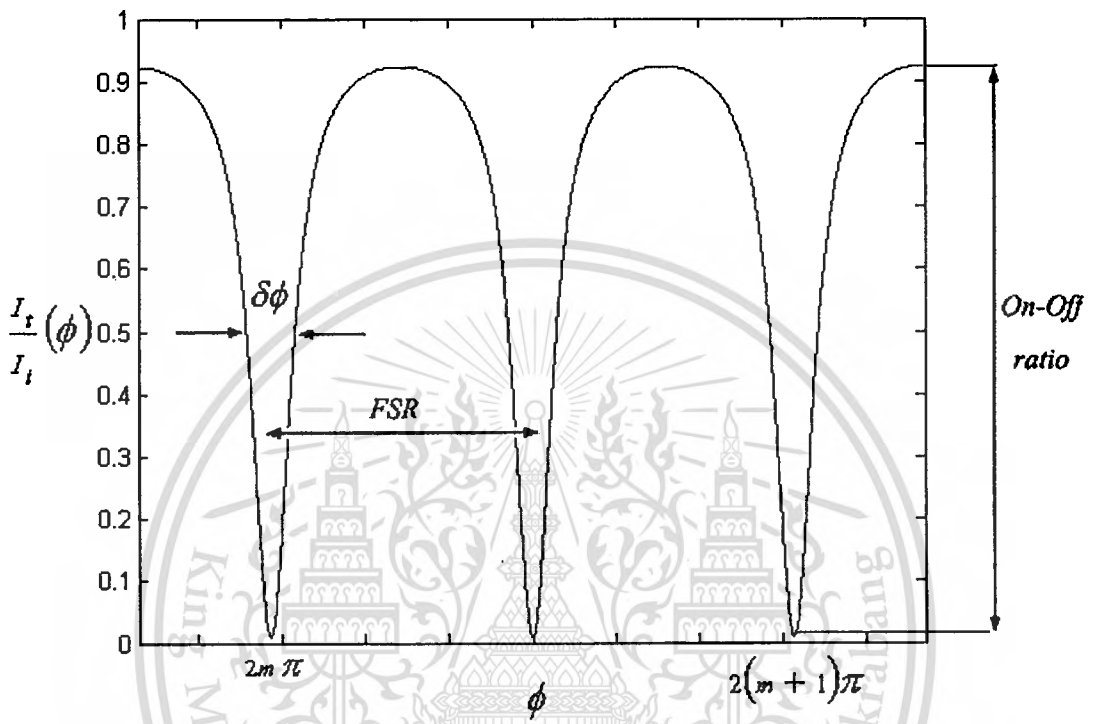

Fig. 2.2 Transmission characteristic of a single ring resonator.

The on-off ratio for the throughput and drop port, which is the ratio of the on-resonance intensity to the off- resonance intensity which is given by:

$$ON - OFF\ ratio = \frac{T_{max(throughput\ port)}}{T_{min(drop\ port)}}. \tag{2.10}$$

The on-off ratio will become maximum if

$$T_{min} = 0 \Rightarrow x = y \Rightarrow \alpha = -\frac{1}{L} \cdot \ln\left(\frac{1-\kappa}{D^2}\right). \tag{2.11}$$

This relationship is also referred to as the critical coupling. The maximum on-off ratio [$\frac{I_t}{I_i}(2m\pi)=0$, Fig. 2.3] can be achieved by varying the coupling factor κ or the intensity attenuation coefficient α (Eq. 2.11). The value of α can only be changed severely by the implementation of an SOA within the ring resonator or using an all-active ring resonator.

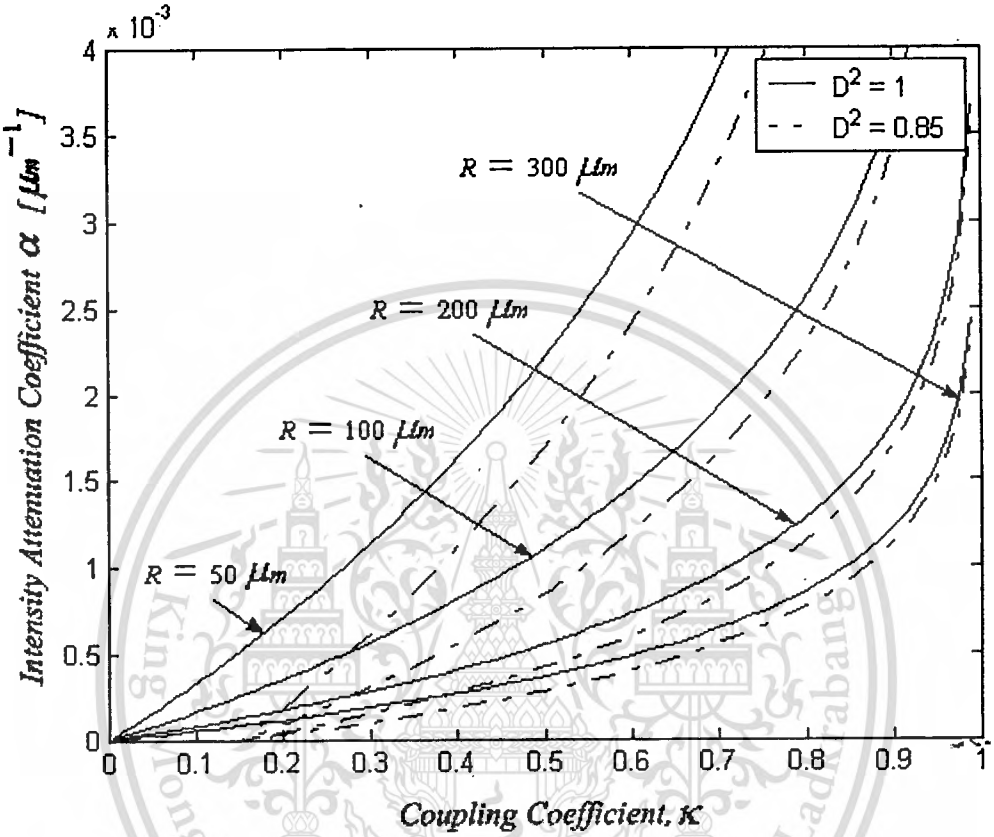

Fig. 2.3 Evaluation of the ideal coupling coefficient κ for a given intensity attenuation coefficient α.

The ideal intensity attenuation coefficient α for single ring resonator to achieve a maximum on-off ratio [$\frac{I_t}{I_i}(2m\pi)=0$], for example, with a radius of R=100 μm, a power coupling coefficient of $\kappa=0.5$, an intensity insertion loss of the coupler of $D^2=85\%$ ($\gamma=15\%$) is taken from the diagram (Fig. 2.4) to be $\alpha=0.0008\,\mu m^{-1}$.

2.2.1 Field Enhancement

At steady state, the field circulating inside the resonator can be also written as

$$E_{r1}=(1-\gamma)^{1/2}\times\left[j\cdot E_i\cdot\sqrt{\kappa}+E_{r1}\cdot\sqrt{1-\kappa}\cdot a\cdot z^{-1}\right]. \quad (2.12)$$

Therefore the ratio of the circulating field to the input field which does not take into account coupling losses ($\gamma = 0$) is given by

$$\frac{E_{r1}}{E_i} = \frac{j\sqrt{\kappa}}{1-\sqrt{(1-\kappa)}\cdot a\cdot z^{-1}}. \tag{2.13}$$

We define the Field Enhancement Factor FE, as the magnitude of the ratio of the circulating field inside the resonator E_{r1}, to the input field E_i, at resonance, i.e., $\phi = 0$. The FE is thus given by

$$FE = \left|\frac{E_{r1}}{E_i}\right|_{\phi=0} = \frac{\sqrt{\kappa}}{1-\sqrt{(1-\kappa)}\cdot a}. \tag{2.14}$$

The higher the FE, the higher the built up intensity inside the resonator and thus the lower the amount of input power required to induce nonlinear effects. Therefore, it is very important to understand what factors limit the FE for a given ring resonator. In Fig. 2.4, we plot Eq. (2.14), for different values of the round trip field transmission, a, and field coupling coefficient, κ. As can be seen, the higher the value of a and therefore the lower the round trip loss, the higher the FE obtained by the resonator. Also, for a given value of a, the FE peaks at a maximum then decreases as a function of κ, as we will discuss in the following subsection.

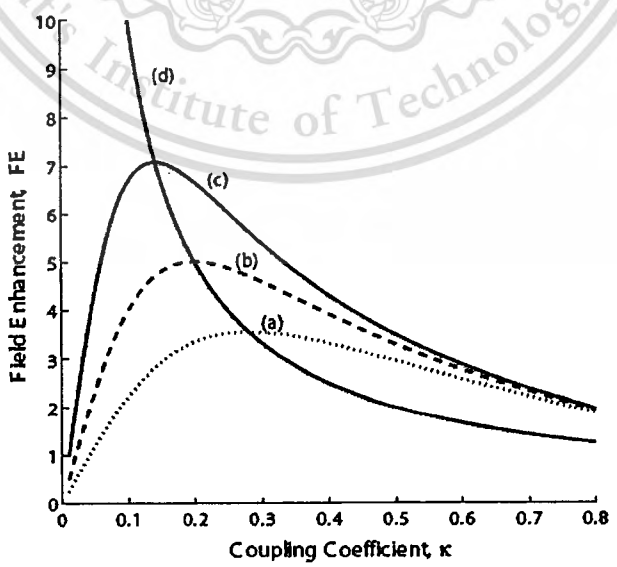

Fig. 2.4 Field Enhancement, FE, versus the coupling coefficient κ, for: (a) $a = 0.96$, (b) $a = 0.98$, (c) $a = 0.99$, and (d) $a = \sqrt{1-\kappa}$

2.2.2 Critical Coupling

The maximum FE that is feasible by a ring resonator can be obtained mathematically by differentiating Eq. (2.14) with respect to κ, and equating the result to 0. Doing the math, we find that this happens when $a = \sqrt{1-\kappa}$, and it yields a maximum FE equal to $1/\kappa$. Moreover, at resonance, the transmission-transfer function, given by Eq. (2.4), has a magnitude of 0, when the above condition is met. That is all the power coupled to the resonator is equal to the power consumed by or lost inside the resonator. This criterion is known as critical coupling and is desirable in some applications where high switching contrast is required. In Fig. 2.5, we plot the throughput transmission and the normalized resonating intensity for a critically coupled ring resonator. At resonance, a complete extinction is achieved for the throughput transmitted intensity. On the other hand, the circulating intensity inside the ring is much higher than the input intensity due to the FE effect.

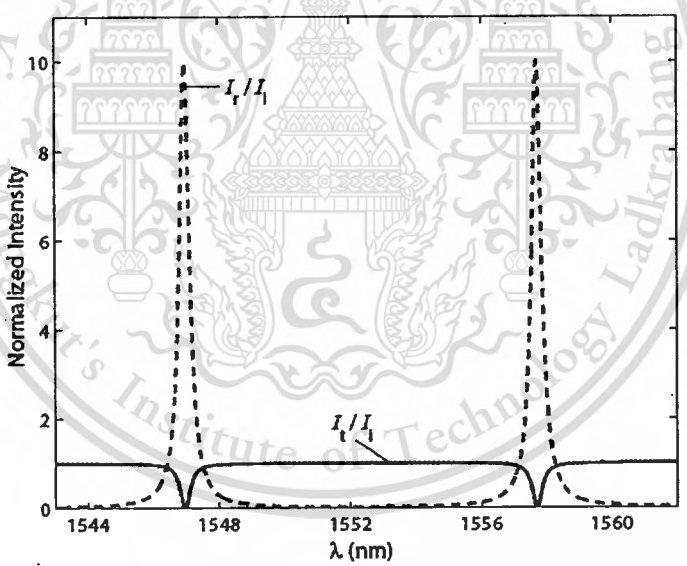

Fig. 2.5 Throughput intensity transmission (solid line) and normalized resonating intensity (dashed line) for a critically coupled ring resonator that has a refractive index of 3.5,diameter of 20 μm, and a power coupling coefficient $\kappa = 10\%$.

2.3 Resonance Characteristics

The performance of resonators can be measured in terms of the resonance width, the free spectral range, the finesse, and the quality factor. Here we derive (approximate) expressions for these characterizing quantities.

2.3.1 Resonance Bandwidth

The resonance bandwidth determines how fast optical data can be processed by a ring resonator. The resonator bandwidth is given by the full width at half maximum (FWHM) of the ring intensity resonance or its 3 dB bandwidth ($\frac{I_t}{I_i}(\phi) = 0.5$). It also is a measure of a sharpness of the resonance. The FWHM of the single ring resonator is given by

$$\delta\phi = \frac{2 \cdot (1 - x \cdot y)}{\sqrt{x \cdot y}}. \tag{2.15}$$

To understand how the bandwidth of the resonator is affected by the coupling coefficient, κ we will consider a critically coupled ring resonator. In such a case, Eq. (2.15) results in

$$\delta\phi = \frac{2 \cdot \kappa}{\sqrt{1 - \kappa}}. \tag{2.16}$$

Therefore, the lower the coupling coefficient, κ the smaller the resonance bandwidth. On the other hand, Eq. (2.14) shows that the lower the coupling coefficient, κ the higher the FE of the resonator.

2.3.2 Finesse, F

The finesse F of the resonator is defined as the ratio of the free spectral range and the full width at half maximum of a resonance. For the Fig. 2.3 using FSR in term of phase is equal to 2π and thus the finesse is given by

$$F = \frac{2\pi}{\delta\phi} = \frac{\pi \cdot \sqrt{x \cdot y}}{(1 - x \cdot y)}. \tag{2.17}$$

The finesse gives the resoling power of the resonator when used as a transmission filter. An interesting fact is that resonator finesse is independent on its dimension or circulating light wavelength. It is only a function of coupling coefficient and internal loss. The finesse of a critical coupling ($x = y$) is given by

$$F_{x=y} = \frac{\pi \cdot y}{1-y^2} = \frac{\pi \cdot \sqrt{1-\kappa}}{\kappa}. \tag{2.18}$$

$$F_{x=y} = \frac{\pi \cdot x}{1-x^2} = \frac{\pi \cdot D\exp^{-\alpha L/2}}{1-D^2\exp^{-\alpha L}}. \tag{2.19}$$

The finesse F depending on the coupling coefficient κ at the point of maximum on-off ratio is shown in Fig. 2.6.

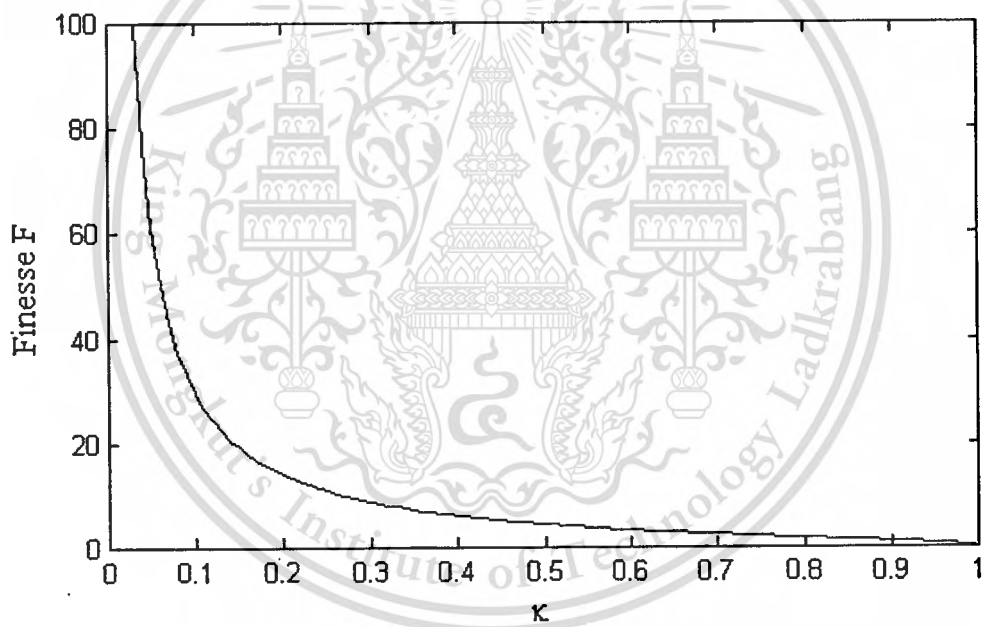

Fig. 2.6 Finesse depending on the coupling coefficient κ at the point of maximum on-off ratio.

The finesse depending on the intensity attenuation coefficient of the ring α at the point of maximum on-off ratio for a ring resonator with $R = 100\ \mu m$ is shown in Fig. 2.7.

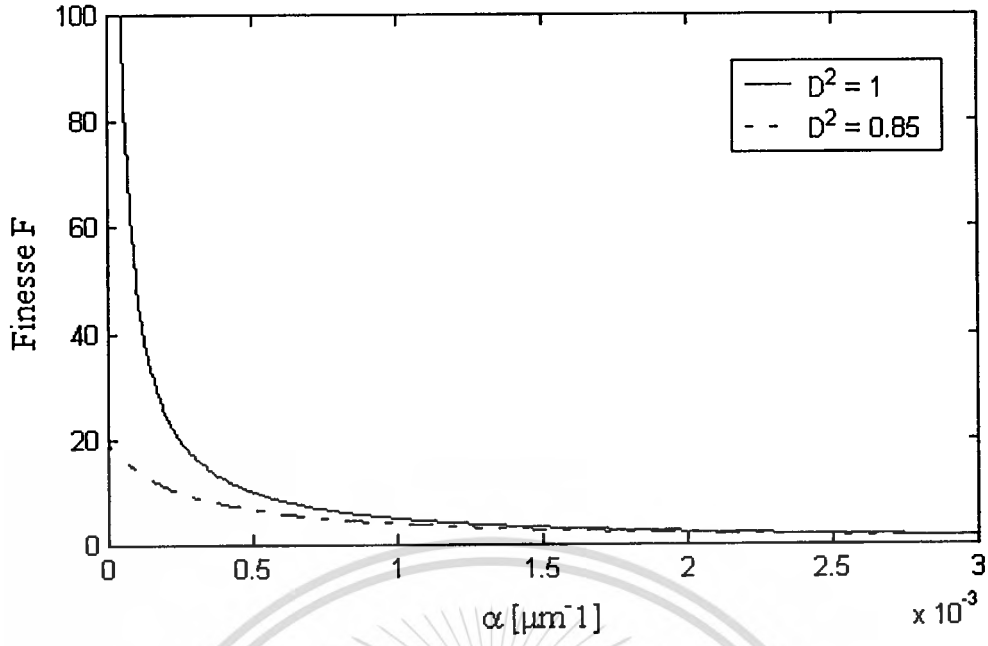

Fig. 2.7 Finesse depending on α at the point of maximum on-off ratio.

A high finesse F > 10 can be realized using a coupling coefficient $\kappa < 0.3$, a coupler with $\gamma < 15\%$ and an intensity attenuation coefficient of the ring $\alpha < 0.0001\ \mu m^{-1}$.

2.3.3 Free Spectral Range, FSR

The frequency spacing between two resonance peaks is call the free spectral range which is calculated as follows: The phase constant which corresponds to $\phi = 2 \cdot m \cdot \pi$ is defined as k. The phase constant which corresponds to $\phi = 2 \cdot (m+1) \cdot \pi$ is defined as $k + \Delta k$.

The frequency shift Δf and the wavelength shift $\Delta\lambda$ are related to variation of the phase constant Δk as $\Delta f = \frac{c}{2\pi} \cdot \Delta k$ and $\Delta\lambda = -(\frac{\lambda^2}{2\pi}) \cdot \Delta k$. The resonance spacing in terms of the frequency f and the wavelength λ are given by

$$\Delta f = \frac{c}{n_{gr} \cdot L}, \tag{2.20}$$

$$\Delta\lambda = \left| -\frac{\lambda^2}{n_{gr} \cdot L} \right|, \tag{2.21}$$

where n_{gr} is the group refractive index, which is defined as

$$n_{gr} \equiv n_{eff} - \lambda \frac{dn_{eff}}{d\lambda}. \tag{2.22}$$

Using $\delta\phi = \delta(k_n \cdot L) = \frac{2\pi}{F}$, the FWHM $\delta\phi$ in term of frequency and wavelength at the resonance peaks are given by

$$\delta f = \frac{c}{F \cdot n_{gr} \cdot L}. \tag{2.23}$$

$$\delta\lambda = \frac{\lambda^2}{F \cdot n_{gr} \cdot L}. \tag{2.24}$$

The finesse can also be calculated using the FSR (Δf or $\Delta\lambda$) and the FWHM (δf or $\delta\lambda$) of a filter and is given by

in the frequency domain:
$$\frac{\Delta f}{\delta f} = \frac{\frac{c}{n_{gr}L}}{\frac{c}{Fn_{gr}L}} = F. \tag{2.25}$$

in the wavelength domain:
$$\frac{\Delta\lambda}{\delta\lambda} = \frac{\frac{\lambda^2}{n_{gr}L}}{\frac{\lambda}{F \cdot n_{gr} \cdot L}} = F. \tag{2.26}$$

2.3.4 Quality Factor

Another value for characterization of ring resonators is the quality factor Q. The Q factor of a resonator is a measure of the sharpness of the resonance. In analogy with electrical circuits, the quality factor of an optical waveguide due its stored energy and the power lost per optical cycle. The Q is defined as

$$Q = \omega \frac{store\ \ energy}{power\ \ loss}, \tag{2.27}$$

where ω is the frequency of light coupled to the resonator. The Q factor of the resonator can be calculated from

$$Q = \frac{f_0}{\delta f} = \frac{\lambda_0}{\delta \lambda}. \tag{2.28}$$

The Q factor is the ratio of the absolute frequency f_0 or absolute wavelength λ_0 to the 3 dB bandwidth (δf or $\delta \lambda$). The shape and the bandwidth (δf or $\delta \lambda$) of the filter response is determined by the Q factor.

The finesse and the Q factor are both important when one is interested in both the FSR (Δf or $\Delta \lambda$) and the 3 dB bandwidth (δf or $\delta \lambda$). They are related by

$$\frac{Q}{F} = \frac{f_0}{\Delta f} = \frac{\lambda_0}{\Delta \lambda}. \tag{2.29}$$

The Q factor depending on the finesse F for a ring resonator with a radius $R = 100\ \mu m$, $50\ \mu m$ and $10\ \mu m$, a group refractive index $n_{gr} = 3.44$ at the wavelength of $\lambda = 1.55\ \mu m$ is shown in Fig. 2.8.

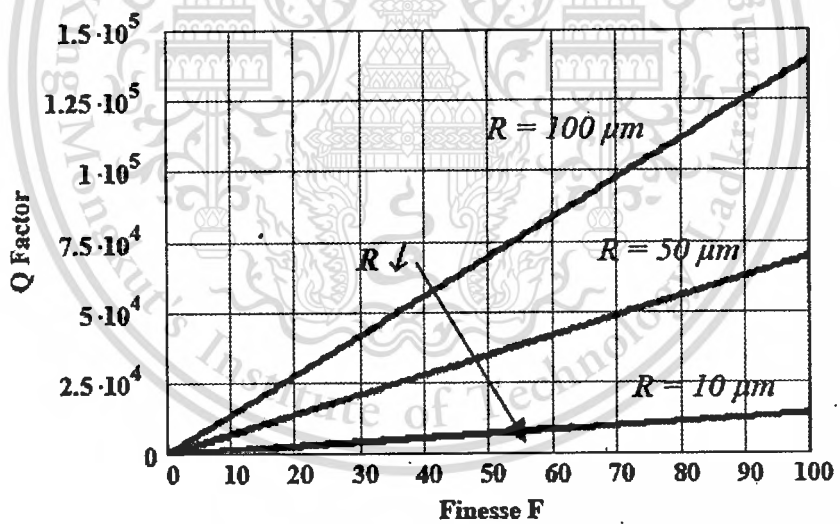

Fig. 2.8 Q factor depending on the finesse F for a specific radius R.

A high finesse (>100) and a low Q factor (<2.5x10^4) is obtained, for example, for ring resonators with a low radius ($R < 20\ \mu m$). A ring resonator for a given specific bandwidth (δf or $\delta \lambda$) can be designed using the following steps

$$\delta f \text{ or } \delta\lambda \xrightarrow{Eq.3.28} Q \xrightarrow{Eq.3.29} F, F \xrightarrow{Eq.3.18, Eq.3.19} \kappa, \alpha \text{ (point of maximum on-off ratio)}$$

High Q cavities can serve for example as building blocks for optical signal processing applications or for laser applications where high quality factors are required. The basic figures for the description of a single ring resonator with one input waveguide have been presented. This model is extended to multiple coupled ring resonators in the next chapters

2.4 Fiber Optic Ring Resonator

The architecture of a nonlinear fiber optics ring resonator as illustrated in Figure 2.9, which is constructed by a single fiber coupler and one ring resonator. We assume that the nonlinearity of the fiber ring is of the Kerr-type, i.e., the refractive index is given by ,

$$n = n_0 + n_2 I = n_0 + (\frac{n_2}{A_{eff}})P, \tag{2.30}$$

where n_0 and n_2 are the linear and nonlinear refractive indexes, respectively. I and P are the optical intensity and optical field power, respectively. The effective mode core area of the fiber is A_{eff} .

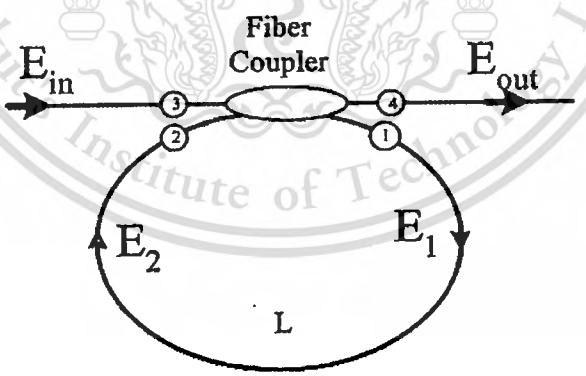

Fig. 2.9 Schematic diagram of FORR with a single fiber coupler.

The input light is launched in port 3 and the output emerges from port 4. It is worth noting that such a device has no reflected wave or no cross-phase modulation occurred at fiber coupler. The ports 1 and 2 are connected with a fiber having a nonlinear refractive index, n_2 and a linear absorption coefficient α . The fiber coupler has an intensity coupling coefficient κ and γ

is a coupling loss for the field amplitude. We assume hereafter (without loss of generality) that the optical fiber ring is on resonance for the operating wavelength in the limit of vanishing incident power, i.e. in the linear case. In addition, we assume that the fiber coupler acts as a point device. The fiber coupler is assumed to be reciprocal and the transmission coefficients for the fields are:

$$t_{34} = t_{21} = (1-\gamma)\sqrt{1-\kappa}, \qquad t_{31} = t_{24} = j(1-\gamma)\sqrt{\kappa}, \\ t_{32} = t_{41} = 0. \tag{2.31}$$

The following relations of the electric fields arise from Eq. (2.30):

$$E_1 = t_{31}E_{in} + t_{21}E_2, \tag{2.32a}$$

$$E_{out} = t_{34}E_{in} + t_{24}E_2. \tag{2.32b}$$

The relation between the electric fields E_1 and E_2, in the stationary state, can be obtained from the nonlinear propagation equation:

$$\frac{\partial E}{\partial z} = j\frac{2\pi n_2}{\lambda}|E|^2 E - \frac{1}{2}\alpha E. \tag{2.33}$$

Integrating the Eq. (2.33) direct, we can thus obtain the following relation:

$$E_2 = E_1\tau\exp(-j\phi) = E_1\tau\exp\{-j(\phi_0 + \phi_{NL})\}, \tag{2.34}$$

Where $\phi_0 = kLn_0$ and $\phi_{NL} = kLn_2|E_1|^2$ are the linear and nonlinear phase shift, $k = 2\pi/\lambda$ is the wave propagation number in a vacuum, and L is the fiber ring resonator length. $\tau = \exp(-\alpha L/2)$ is a one round trip loss in FORR.

It was discovered in 1979 that the nonlinear response of a ring resonator can initiate a period-doubling route to optical chaos. The basic idea consists of recognizing that the dynamics in FORR correspond to that of a nonlinear map round trip inside the FORR. Mathematically, from Esq. (2.32) and (2.34) the map can be written as

$$E_1(t) = j(1-\gamma)\sqrt{\kappa}E_{in} + (1-\gamma)\sqrt{1-\kappa}\tau E_1(t-t_R)\exp(-j\phi). \tag{2.35}$$

$$E_{n+1} = j(1-\gamma)\sqrt{\kappa}E_{in} + (1-\gamma)\sqrt{1-\kappa}\tau E_n \exp(-j\phi), \tag{2.36}$$

Where the subscript "n" denotes the number of round trips inside the FORR. Using Eq. (2.36), the nonlinear map can be iterated for a given value of the input power P_{in} ($\alpha|E_{in}|^2$). The results show that the output of the FORR can become time dependent even for a CW input. Moreover, the output becomes chaotic following a period-doubling route in a certain range of input parameters.

The nonlinear phenomenon of optical bistability has been studied in non-fiber resonators since 1976 by placing the nonlinear medium inside a cavity formed by using multiple mirrors. The single-mode fiber was used in 1983 as the nonlinear medium inside a ring cavity. Since then, the study of nonlinear phenomena in fiber ring resonators has remained a topic of considerable interest. Consider at steady state, from the Eq. (2.35), we have

$$E_1 = j(1-\gamma)\sqrt{\kappa}E_{in} + (1-\gamma)\sqrt{1-\kappa}\tau\exp(j\phi)E_1. \tag{2.37}$$

While the output field at steady state as

$$E_{out} = (1-\gamma)\cdot E_{in}\left[\sqrt{1-\kappa} - \frac{(1-\gamma)\kappa\tau\exp(j\phi)}{1-(1-\gamma)\sqrt{1-\kappa}\tau\exp(j\phi)}\right]. \tag{2.38}$$

Thus the normalized of the light field from Eq. (2.38) can be expressed as

$$\left|\frac{E_{out}}{E_{in}}\right|^2 = (1-\gamma)^2\left[1 - \frac{\kappa\left[1-(1-\gamma)^2\tau^2\right]}{1+(1-\gamma)^2(1-\kappa)\tau - 2(1-\gamma)\sqrt{1-\kappa}\tau\cos\phi}\right]. \tag{2.39}$$

Esq. (2.36) and (2.39) are mathematical relations are used for characterizing a nonlinear effects such as bifurcation, chaos, and optical bistability, respectively.

CHAPTER 3

ERBIUM-DOPED FIBER AMPLIFIERS

In this chapter we will develop and review the fundamentals needed to model gain in erbium-doped fiber amplifiers. The underpinning of the gain process consists of coupled atomic population and light flux propagation equations. We will treat the three-level system appropriate for erbium-doped fiber amplifiers at 1.5 μm. We will discuss calculations of the gain in both the small signal and saturation regimes to reach an intuitive understanding of the gain process. Then we will show how the three-level system can be reduced, with certain assumptions, to an equivalent two-level system. The importance of the absorption and emission cross sections, and the difference between the two at a given transition wavelength, will be highlighted. We will cover the concept of the overlap parameter, representing the geometric overlap between the transverse erbium ion distribution and the transverse profile of the light intensity. We will then outline the importance of amplified stimulated emission and the fundamental mechanism by which it is intertwined into all aspects of the amplification process.

3.1 Amplification in three-level systems -basics

3.1.1 Three-Level Rate Equation

The most simple treatment of the erbium-doped fiber amplifier starts out by considering a pure three-level atomic system. Most of the important characteristics of the amplifier can be obtained from this simple model and its underlying assumptions. An added complication- possible stimulated emission at the pump wavelength-will be treated in

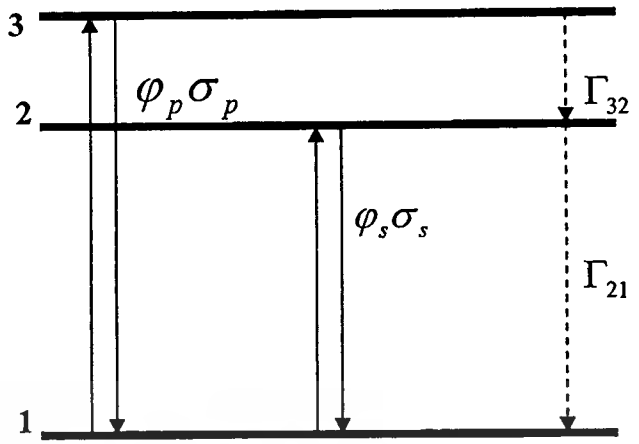

Fig. 3.1 The three-level system used for the amplifier model.

The transition rates between levels 1 and 3 are proportional to the populations in those levels and to the product of the pump flux ϕ_p and pump cross section σ_p. The transition rates between levels 1 and 2 are proportional to the populations in those levels and to the product of the signal flux ϕ_s and signal cross section σ_s. The spontaneous transition rates of the ion (including radioactive and nonradiative contributions) are given by Γ_{32} and Γ_{21}.

We consider a three-level system as depicted in Fig. 3.1, with a ground state denoted by 1, an intermediate state labeled 3 (into which energy is pumped), and state 2. Since state 2 often has a long lifetime in the case of a good amplifier, it is sometimes referred to as the metastable level. State 2 is the upper level of the amplifying transition and state 1 is the lower level. The populations of the levels are labeled N_1, N_2, and N_3 This three-level system is intended to represent that part of the energy level structure of Er^{3+} that is relevant to the amplification process. To obtain amplification, we need a population inversion between states 1 and 2 , and since state 1 is also the ground state, at least half of the total population of erbium ions needs to be excited to level 2 to have population inversion. This raises the threshold pump power needed for amplification and is a known drawback of three-level laser and amplifier systems.

One can take particular advantage, in the case of the erbium-doped fiber amplifier, of the fact that the light fields are confined in a core of very small dimension. The light intensities reached are thus very high, over long distances, and population

inversion is achieved with relatively small pump powers. We will initially consider the problem to

Be one-dimensional. That is, we assume that the pump and signal intensities as well as the erbium ion distribution are constant in the transverse dimensions, over an effective cross-sectional area of the fiber. We will consider in the next chapter the effects of the transverse variation in the light-field intensities and erbium ion distribution on the performance of the amplifier.

The incident light intensity flux at the frequency corresponding to the 1 to 3 transition (in number of photos per unit time per unit area) is denoted by ϕ_p and corresponds to the pump. The incident flux at the frequency corresponding to the 1 to 2 transition (in photons per unit time per unit area) is denoted by ϕ_s and corresponds to the signal field. The change in population for each level arises from absorption of photons from the in cadent light field, from spontaneous and stimulated emission, and from other pathways for the energy to escape a particular level. In particular, we write as Γ_{32} the transition probability from level 3 to level 2. This is the sum of the nonradiative and radioactive transition probabilities, and in practice, for the most typical cases, is mostly nonradiative. Γ_{21} is the transition probability from level 2 to level 1. In the case of the Er^{3+} $^4I_{13/2}$ (level 2) to $^4I_{15/2}$(level 1) transition, Γ_{21} is mostly due to irradiative transitions. This is due to the fact that fact that there are, for Er^{3+}, no intermediate states between levels 1 and 2 to which ions excited to level 2 can relax. We define $\Gamma_{21} = 1/\tau 2$. Where $\tau 2$ is the lifetime of level 2. The typical values of the transition rates between levels for Er^{3+} doped in glasses.

We denote the absorption cross section for the 1 to 3 transition by σ_p. and the emission cross section for the 2 to 1 transition by σ_s. We will assume for the time being that the absorption and emission cross sections we consider are those for transitions between individual no degenerate states and are thus equal. We will consider in Section 3.2 the more practical case of erbium levels that consist of a set of states, and where the absorption and emission cross sections are different, as they incorporate information on the thermal population distribution.

The rate equations for the population changes are written as

$$\frac{dN_3}{dt} = -\Gamma_{32}N_3 + (N_1 - N_3)\,\phi_p\,\sigma_p \tag{3.1}$$

$$\frac{dN_2}{dt} = -\Gamma_{21}N_2 + \Gamma_{32}N_3 - (N_3 - N_1)\,\phi_s\,\sigma_s \tag{3.2}$$

$$\frac{dN_1}{dt} = -\Gamma_{21}N_2 - (N1-N3)\,\phi_p\,\sigma_p + (N_2 - N_1)\,\phi_s\,\sigma_s \tag{3.3}$$

In a steady-state situation, the time derivatives will all be zero,

$$\frac{dN_1}{dt} = \frac{dN_2}{dt} = \frac{dN_3}{dt} = 0 \tag{3.4}$$

And the total population N is given by

$$N = N_1 + N_2 + N_3 \tag{3.5}$$

Using Eq.(3.1), we can write the population of level 3 as

$$N_3 = \frac{1}{1 + \Gamma_{32}/\phi_p\sigma_p}\,N_1 \tag{3.6}$$

When Γ_{32} is large (fast decay from level 3 to level 2) compared to the effective pump rate into level 3, $\phi_p\sigma_p$, N_3 is very close to zero, so that the population is mostly in levels 1 and 2. Using Eq.(3.6) to substitute for N_3 in Eq. (3.2) we obtain

$$N_2 = \frac{(\phi_p\sigma_p/\Gamma_{32}) + \phi_s\sigma_s}{\Gamma_{21} + \phi_s\sigma_s}\,N_1 \tag{3.7}$$

We then make use of Eq. (3.5) derive the populations N_1 and N_2 and the population inversion N_2-N_1 :

$$N_2 - N_1 = \frac{\phi_p\sigma_p - \Gamma_{21}}{\Gamma_{21} + 2\phi_s\sigma_s + \phi_p\sigma_p}\,N \tag{3.8}$$

The condition for population inversion, and thus for gain on the 2 to 1 transition (as summing no background loss), is that $N_2 \geq N_1$. The threshold corresponds to $N_1 = N_2$ and results in the following expression for the pump flux required :

$$\phi_{th} = \frac{\Gamma_{21}}{\sigma_p} = \frac{1}{\tau_2 \sigma_p} \tag{3.9}$$

In a situation where the signal intensity is very small, and the decay rate Γ_{32} is large compared to the transition rate induced by the pump field, $\phi_p \sigma_p$, we can thus write the population inversion as :

$$\frac{N_2 - N_1}{N} = \frac{\phi'_p - 1}{\phi'_p + 1} \tag{3.10}$$

Where

$$\phi'_p = \frac{\phi_p}{\phi_{th}} \tag{3.11}$$

We plot the fractional population inversion, as given by Eq.(3.10), in Fig.3.2, Below the pump threshold the inversion is negative ; above the pump threshold it is positive. When the inversion is negative, there are more absorptive transitions than emissive transitions at the signal wavelength, and the signal sees negative gain, i.e., attenuation. Conversely, when the inversion is positive, the signal experiences positive gain as it traverses the excited medium (summing no background attenuation).

The pump intensity, in units of energy of energy per unit area per unit time, is expressed as $I_p = h\nu_p \phi_p$. The threshold pump intensity s then given very simply by the expression:

$$I_{th} = \frac{h\nu_p \Gamma_{21}}{\sigma_p} = \frac{h\nu_p}{\sigma_p \tau_2} \tag{3.12}$$

This equation is intuitively easy to understand. The higher σ_p is, the higher the probability that a pump photon is absorbed, which lowers the number of pump photons necessary to guarantee that enough are absorbed to reach threshold. In addition, the longer τ_2 is, the longer the energy stays in the reservoir formed by level 2, and, as a

result, less pump photons are needed per unit time to keep energy in level 2, The conditions for low pump threshold are thus easily summarized as :

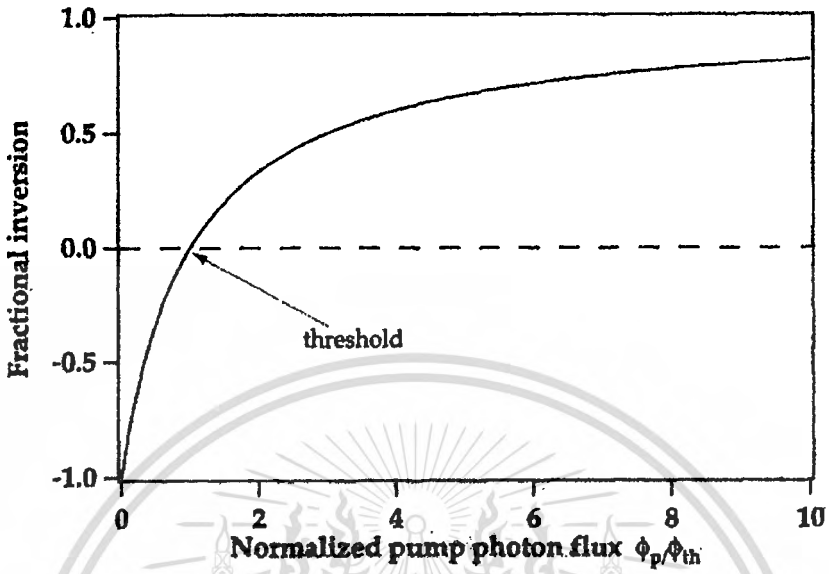

Fig.3.2 Fractional population inversion (N_2 - N_1) in a three-level system.The threshold corresponds to $\phi p = \phi th$ as defined in Eq.(3.9)

* high absorption cross section
* long lifetime of the detestable level

For erbium, the situation is particularly propitious from the point of view of τ_2, as the lifetime has the very large value of approximately 10 ms in silica glass.

We can estimate I_{th} by using some typical values for the erbium ion constants. We consider a pump in wavelength of 980 nm, $\sigma_p = 2 \times 10^{-21}$ cm^2, and a τ_2 lifetime of 10 ms to obtain $I_{th} \sim 10$ kW/cm^2. Assuming that this pump intensity is distributed uniformly over an effective area (A_{eff}) of 5 μm^2 (the core area for a small-core, erbium-doped single-mode fiber), this corresponds to power threshold $P_{th} = I_{th}\ A_{eff} \approx 0.5$ mW. Note that this corresponds to rendering transparent only an infinitesimally short length of erbium-doped medium. This ultra low threshold dramatically illustrates one of the main advantages of erbium-doped single-mode fiber amplifiers : a low pump threshold for gain, easily obtained with electrically pumped diode lasers.

3.1.2 Small Signal Gain

In this subsection we will calculate the gain or loss of pump and signal light propagating through a medium constituted by the ions characterized by the three-level system considered in the previous subsection.

We now consider that N, N_1, N_2, are N_3 densities of populations, in unit of number of ion per unit volume. Two light fields travel through the medium, interacting with the ions, and have insensate I_s (the signal field) and I_p (the pump field). The photon fluxes are given by :

$$\phi s = \frac{I_s}{h\nu_s} \tag{3.13}$$

and

$$\phi p = \frac{I_p}{h\nu_p} \tag{3.14}$$

We will treat the propagation of the signal along a single direction z (the axis of the fiber) as a one-dimensional problem, which is a simplification of the three-dimensional character of the erbium ion distribution in the fiber core and of the light modes. We will extend the discussion to the three-dimensional aspect of the field propagation, which involves the variation of the signal and pump intensities in the plane transverse to the axis of the fiber.

In the one-dimensional case, the light field intensities are derived from the light field powers by the following simplified relationship:

$$I(z) = \frac{P(z)\Gamma}{A_{eff}} \tag{3.15}$$

Where Γ is the overlap factor, representing the overlap between the erbium ions and the mode of the light field, and A_{eff} is the effective cross-sectional area of the distribution of erbium ions. The overlap factor and effective cross section. Essentially states that the intensity of the field at a point z will be taken to its cross-sectional average, computed as the amount of power traveling through the erbium-doped region of the fiber, divided by its cross-sectional area.

We will also assume in the following discussion that both pump and signal beams are propagating in the same direction, i.e., a co propagating configuration as opposed to a counter propagating configuration.

The fields will be attenuated or amplified after an infinitesimal length dz by the combined effects of absorption arising from ions in their ground state (N_1) and stimulated emission from ions in the excited state (N_2 and N_3)

$$\frac{d\phi_s}{dz} = (N_2 - N_1)\sigma_s\phi_s \tag{3.16}$$

$$\frac{d\phi_p}{dz} = (N_3 - N_1)\sigma_p\phi_p \tag{3.17}$$

This leads, after some calculation, to the following equation for the signal intensity growth (or decay, as the case may be):

$$\frac{dI_s}{dz} = \frac{\frac{\sigma_p I_p}{h\nu_p} - \Gamma_{21}}{\Gamma_{21} + 2\frac{\sigma_s I_s}{h\nu_s} + \frac{\sigma_p I_p}{h\nu_p}}\sigma_s I_s N \tag{3.18}$$

We can write an equation for the attenuation of the pump intensity as

$$\frac{dI_p}{dz} = \frac{\Gamma_{21} + \frac{\sigma_s I_s}{h\nu_s}}{\Gamma_{21} + 2\frac{\sigma_s I_s}{h\nu_s} + \frac{\sigma_p I_p}{h\nu_p}}\sigma_p I_p N \tag{3.19}$$

From Eq. (3.18),it is clear that the condition for gain for the signal field is that

$$I_p \geq I_{th} = \frac{h\nu_p}{\sigma_p \tau_2} \tag{3.20}$$

Where we again used $\Gamma_{21} = 1/\tau 2$ and I_{th} is the pump threshold intensity for gain at the signal wavelength. This is equivalent to the condition derived above for population inversion.

We can write the equation in a somewhat simpler fashion by defining the intensities in units of the pump threshold. These "normalized" intensities are given by

$$I'_p = \frac{I_p}{I_{th}} \tag{3.21}$$

$$I'_s = \frac{I_s}{I_{th}} \tag{3.22}$$

We further define the quantity η as

$$\eta = \frac{h\nu_p}{h\nu_s}\frac{\sigma_s}{\sigma_p} \tag{3.23}$$

And the saturation intensity $I_{sat}(z)$ as

$$I_{sat}(z) = \frac{1+I'_p(z)}{2\eta} \tag{3.24}$$

We can then write the propagation equations for the normalized intensities as

$$\frac{dI'_s(z)}{dz} = \frac{1}{1+I'_s(z)/I_{sat}(z)}\left(\frac{I'_p(z)-1}{I'_p(z)+1}\right)\sigma_s I'_s(z)N \tag{3.25}$$

And for the pump

$$\frac{dI'_p(z)}{dz} = \frac{1+\eta I'_s(z)}{1+2\eta I'_s(z)+I'_p(z)}\sigma_p I'_p(z)N \tag{3.26}$$

Eq. (3.25) and (3.26) determine the behavior of erbium-doped fiber amplifiers, at the simplest level. As we shall discuss in the following sections and chapters, modifications

will need to be made to this system of equations to accurately model real erbium-doped fibers. Nevertheless, the basic characteristics of three-level fiber amplifiers can be understood from the above equations. We now explore Eq. (3.25) and (3.26) in more detail.

The signal propagation equation will lead to gain only if $I_p \geq I_{th}$. This is the expected threshold condition. When the pump intensity is less than threshold, the signal is attenuated; when it is larger, the signal is amplified. Under the conditions of small signal gain, where $I_s' << I_{sat}$ (this condition is satisfied when the signal is weak and the pump is strong,) and assuming for simplicity that the pump is constant as a function of z (the fiber is uniformly inverted), the signal propagation equation is easily integrated to yield the signal as a function of position along the fiber;

$$I_s'(z) = I_s'(0) \exp(\alpha_p z) \tag{3.27}$$

Where we defined the gain coefficient α_p as

$$\alpha_p = \frac{I_p' - 1}{I_p' + 1} \sigma_s N \tag{3.28}$$

The signal grows exponentially, with a coefficient proportional to the signal emission cross section and the degree to population inversion. The latter is determined by the pump intensity relative to threshold. When the pump intensity is very strong and several times the threshold, such that the erbium ions are all inverted, the gain coefficient becomes approximately

$$\alpha_p = \sigma_s N \tag{3.29}$$

The small signal gain per unit length of fiber for a strong pump is determined very simply by the amount of erbium and the signal emission cross section. This implies that in the case of Er^{3+} doped in an Al-Ge silica fiber, since the emission cross section Is equal to the absorption cross section, near 1535 nm, the 1535 nm small signal gain is roughly equal to the 1535 nm small signal attenuation under strong pumping conditions.

In practice this does not happen, due to the presence of amplified spontaneous emission, which robs the gain at the expense of the signal.

3.1.3 Saturation Regime

Eq. (3.28) loses its validity when the signal grows to a large enough value and enters what is known as the saturation regime. This occurs when Is becomes comparable in value to I_{sat}. The signal growth is then damped by the saturation factor $1/(1+I_s'/I_{sat})$. In fact, when I_s' becomes very large and its ration to I_{sat} becomes large compared to unity. The growth of the signal is determined by the approximate equation

$$\frac{dI_s'}{dz} = I_{sat}\left(\frac{I_p'-1}{I_p'+1}\right)\sigma_s N \tag{3.30}$$

So that now the signal growth is linear. The two regimes of signal growth are clear in the graph of Fig. 3.3, which plots the gain in dB of a weak signal as a function of pump power. The gain, in dB, of the signal after a length L of fiber is defined as $G = 10\log(I_s(z = L)/I_s(z = 0))$. Fig. 3.3 is derived using some typical values for an alumino - germano - silica erbium-doped fiber of length 15 m, with a signal at 1550 nm with a launched power of -40 dBm, an a pump of wavelength of 980 nm. Also shown is the gain obtained when modeling the fiber with the added effect of amplified spontaneous emission (ASE).The effect of ASE is to reduce the available gain for the signal field. In the case shown, the ASE begins significantly impairing the gain process above signal levels of approximately 20 dB.

An interesting phenomenon is that the saturation power I_{sat} is not a constant, but instead increases linearly with pump power. This is expected to occur for a three-level laser system. It arise from the following fact, In a three-level laser, ions driven down from the excited level 2 by stimulated emission by the signal are immediately available for pump absorption and can be returned to the excited level almost "instant tenuously". Given a high enough pumping rate. Maintaining level of inversion in the presence of a high signal power yields a high saturation value for the signal.

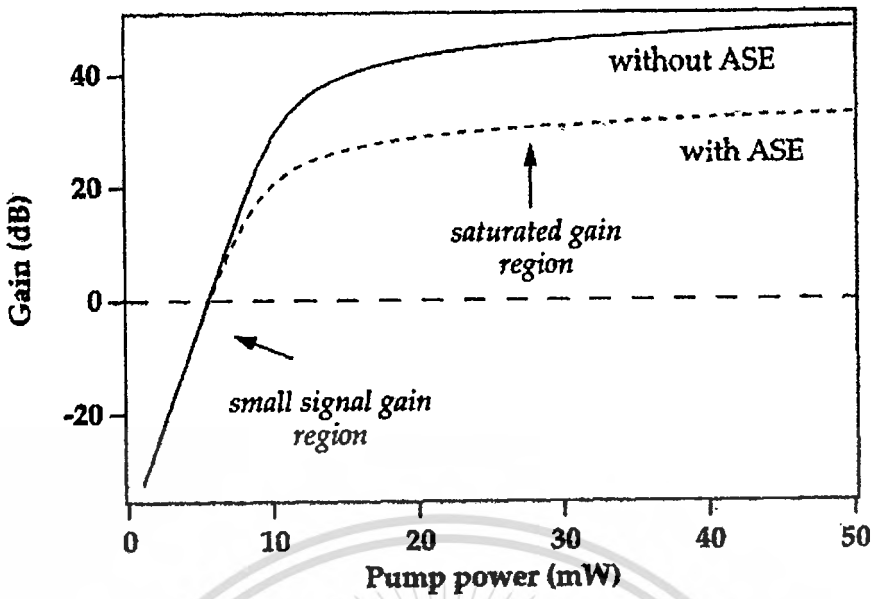

Fig. 3.3 Signal gain (in dB) at 1550 nm as a function of pump power at 980 nm.

For a typical erbium-doped fiber (15 m length of fiber), from numerical integration of the pump and signal propagation equations. The dashed curve shows the computed gain when amplified spontaneous emission is included in the simulation of the gain of the fiber amplifier ; the solid curve includes only the pump and small signal of power-40 dBm. At low pump powers the amplifier is in the small signal gain regime; at higher powers when it is strongly inverted the gain is saturated.

The experimentally determined saturation output power is defined as the signal output power at which the gain has been reduced (compressed) by 3 dB. The saturation output power is higher at 1550 nm than at 1530 nm because the emission cross section is lower for the latter, and the saturation output power is proportional to the inverse of the emission cross section.

3.1.4 Optimal Length for a Fiber Amplifier

For a given pump power, to obtain the maximum amount of gain for a given erbium concentration in the fiber core, the fiber length should be increased to the point at which the pump power becomes equal to the intrinsic pump threshold (for the model without ASE considered up to the present point). For axial point z, along the length of the fiber, prior to that point the gain is positive, after that point the gain is negative, and so the fiber should be terminated at the point where the pump power has decreased to the

threshold level. This determines the optimal length of the fiber. This length is optimal only in the sense that the small signal gain of the amplifier is maximized. When ASE is included the optimum length for gain is determined by maximizing the signal gain in the presence of forward and backward ASE, which is also a function of the length.

When we need to optimize another parameter, say the noise figure of output saturation power, the optimal length determination will proceed differently. For example. It can be helpful to use an amplifier length such that one is operating in the saturation regime where fluctuations in the pump source power do not have a large effect on the

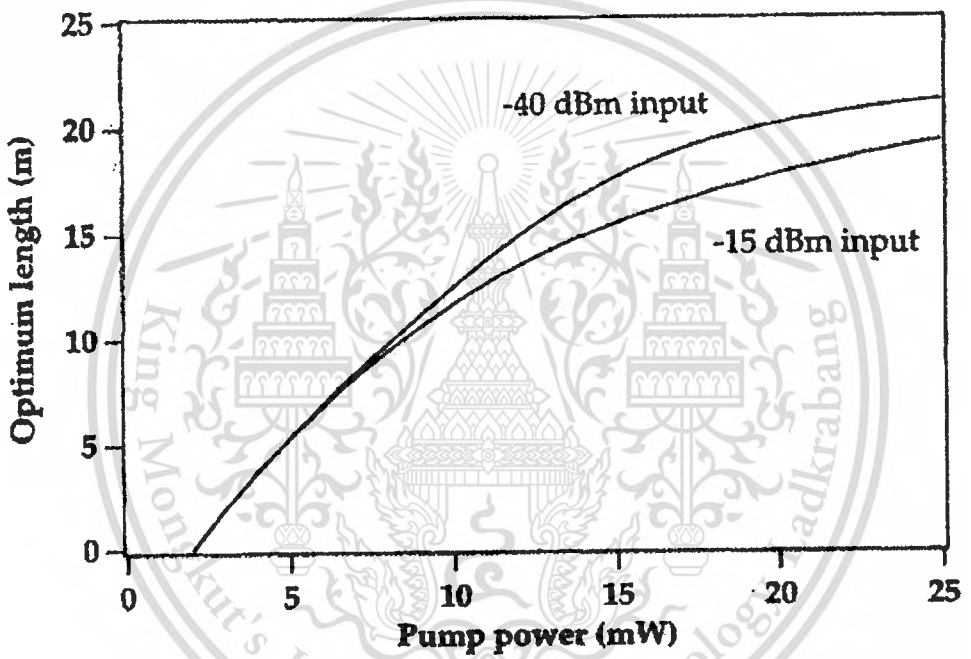

Fig. 3.4 Optimal fiber length (in m) for gain at 1530 nm as a function of pump power. For signal inputs of -40 and -15 dBm, from numerical simulations of an erbium-doped fiber pumped at 980 nm.

Gain, as would be the case in the small signal gain regime. We plot in Fig 3.4 the optimal length for small signal gain for two different small signal inputs. The optimum length is 0.up until the point at which the pump power is equal to the power needed to render transparent an infinitesimal length of fiber, i.e., p_{th}.

3.2 Reduction of the three-level system to the two-level system

3.2.1 Validity of the Two-Level Approach

The energy levels of rare earth ions are composed of relatively well-separated multiples, each of which I made up of a certain number of broadened individual levels. We assume that the pumping level 3 belongs to a multiple different than that of level 2, and we assume that there is rapid relaxation from level 3 to level 2, For all practical purposes, the population in level 3 is then effectively zero and the rate equations involve only the two levels 1 and 2, with level 3 being involved only via the value of the pump abs absorption cross section from level 1 to level 3. Examples of pump wavelengths in this case are 0.98 μm, 0.80μm, 0.65 μm, and 0.54 μm.

In certain pumping configurations, level 3 can be identical to level 2 in the sense that the upper pump level and the upper amplifier level belong to the same multiple.

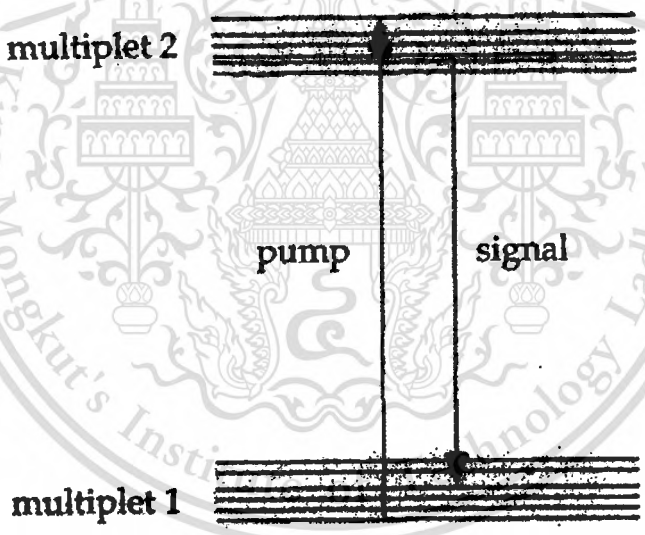

Fig. 3.5 Energy levels of a two-multiple system.

Where the pumping state 3 is higher-lying state of multiplet 2, and the signal is resonant with a lower energy transition between the two multiples, as compared to the pump transition.

This particular case is that of a 1.48 μm pluming wavelength and is depicted in Fig. 3.5. In this case, the population of level 3 will not necessarily be equal to zero. At all times, there will be thermal equilibrium established within a given multiple, assuming that the thermal equilibration time is very short compared to the overall multiple lifetime

(which is governed by decay to lower-lying multiples). Thus, the pumping level3, depending on its energy separation from the bottom of the multiple, will have some finite thermal population. There will then be stimulated emission at the pump frequency as well as at the signal frequency, the amount of which depends on the thermal population of the various states involved as well as the strength of their interaction with a light field.

The behavior of the entire system can be represented through the absorption and emission cross sections . The difference in spectral shape between the absorption and emission spectra is due to the thermal distribution of energy within the multiplets. The absorption and emission information. For example, if level 3 is high above the bottom of the multiplet and its thermal occupation low, then its emission cross section for emission to the bottom of the ground multiple will be relatively small, indicating the low probability emission at that frequency. The absorption cross section at that frequency will be significantly higher, since most of the population of the ground multiplet will be near the bottom of the multiplet and, as a consequence, available for transitions to level 3.

Based on the previous discussion, we will refer only to the total populations of levels 1 and 2, N1 and N2, and use the cross sections to model the system's interaction with the pump and signal fields. In general, the emission and absorption cross sections will be related by the McCumber . The case where level 3 belongs to a higher-lying multiplet can be reduced to the two-level picture just described by simply setting the pump emission cross section to zero, which effectively accounts for the fact that the population of level 3 is in this case equal to zero.

3.2.2 Generalized Rate Equations

Having reduced the three-level system to an effective two-level system, we can write the rate equations so as to involve only the total population densities of multiplets 1 and 2.

$$\frac{dN_2}{dt} = -\Gamma_{21}N_2 + (N_1\sigma_s^{(a)} - N_2\sigma_s^{(e)})\varphi s - (N_2\sigma_p^{(e)} - N_1\sigma p(a)\phi_p$$

$$\frac{dN_1}{dt} = -\Gamma_{21}N_2 + (N_2\sigma_s^{(e)} - N_1\sigma_s^{(a)})\phi_s - (N_1\sigma_p^{(e)} - N_2\sigma_p^{(e)})\phi_p \qquad (3.31)$$

Where $\sigma s^{(a)}$, $\sigma s^{(e)}$, $\sigma p^{(a)}$ and $\sigma p^{(a)}$ represent the signal pump absorption and emission cross sections, respectively. Since the total population density N is given by

$$N = N_1+N_2 \tag{3.32}$$

We have

$$\frac{dN_1}{dt} = -\frac{dN_2}{dt} \tag{3.33}$$

And, only one of the equations from system 3.31 is an independent equation. We can calculate N_2, for example, in terms of the signal and pump intensities. N_1 is then simply given by $N-N_2$. We find from Eq. (3.31), for the case of pump field and one signal field, that the population density N_2 (z), as a function of position z along the fiber, is given by

$$N_2(z) = \frac{\frac{\tau\sigma_s^{(a)}}{h\nu_s} I_s(z) + \frac{\tau\sigma_p^{(a)}}{h\nu_p} I_p(z)}{\frac{\tau(\sigma_s^{(a)}+\sigma_s^{(e)})}{h\nu_s} I_s(z) + \frac{\tau(\sigma_p^{(a)}+\sigma_p^{(e)})}{h\nu_p} I_p(z) + 1} N \tag{3.34}$$

In general, we will assume that N is independent of z. The pump and signal propagation equations are then written, in a very similar fashion, as

$$\frac{di_p(z)}{dz} = (N_2\sigma_p^{(e)} - N_1\sigma_p^{(a)})I_p(z)$$

$$\frac{di_s(z)}{dz} = (N_2\sigma_s^{(e)} - N_1\sigma_s^{(a)})I_s(z) \tag{3.35}$$

Stimulated emission from level 2 contributes to field growth, absorption from level 1 contributes of field attenuation. The equations needed simulate the simulate the amplifying properties of the fiber are thus the populstion equation and the propagation equations. One for each field. The condition for population inversion, $N_2-N_1 > 0$, in the presence of a small signal field, corresponds to the pump being greater than the than the threshold value :

$$I_{th} = \frac{h\nu_p}{(\sigma_p^{(a)} - \sigma_p^{(e)})\tau_2} \tag{3.36}$$

The pump threshold that corresponds to signal gain at the signal wavelength ($dI_s/dz > o$) is slightly different and is equal to

$$I_{th} = \frac{h\nu_p}{\tau_2} \frac{1}{\sigma_p^{(a)} \left(\frac{\sigma_p^{(e)}}{\sigma_s^{(a)}} \right) - \sigma_p^{(e)}} \tag{3.37}$$

The equations above can be easily generalized to the case of multiple signals and multiple pumps. For the case of several signals s_i and several pumps p_i, the population equation becomes

$$N_2(z) = \frac{\sum_{s_i} \frac{\tau \sigma_{si}^{(a)}}{h\nu_{si}} I_{si}(z) + \sum_{p_i} \frac{\tau \sigma_{pi}^{(a)}}{h\nu_{si}} I_{pi}(z)}{\sum_{s_i} \frac{\tau(\sigma_{si}^{(a)} + \sigma_{si}^{(e)})}{h\nu_{si}} I_{si}(z) + \sum_{s_i} \frac{\tau(\sigma_{pi}^{(a)} + \sigma_{pi}^{(e)})}{h\nu_{pi}} I_{pi}(z) + 1} N \tag{3.38}$$

The field propagation equations are identical to those of Eq.(3.35), with the appropriate cross sections. Such multilingual systems of equations of equations will be used when computing, for example, the spectral distribution of the ASE or the amplification of multiple-signal channels in a WDM system.

3.3 EDFA Design Issues

The main parameters in the design of an EDFA include the fiber glass material, the waveguide characteristics of the fiber, the erbium concentration profile, fiber length, pump sources, and any passive or active components such as couplers, isolators, filters, etc. The design of the amplifier depends on the intended application. However, the primary design goals are high gain, high output power, low noise figure, flatness of the gain spectrum, reliability, etc. The importance of each of these parameters depends on the particular application type. For example, a single-channel inline amplifier requires high power and low noise figure, but the gain flatness is

unimportant. By contrast, in the design of a WDM amplifier, flat gain profile is the most important parameter. Power amplifiers require high gain and output power, and may not have constraints on the noise figure and gain flatness. Analog amplifiers are the most demanding since all the described parameters are important to amplify the signal keeping the waveform.

3.3.1 Pumping configuration

Three different pumping configurations are possible for pumping a length of erbium-doped fiber : co-propagating pump and signal, counter-propagating pump and signal, and bidirectional pumping as shown in Fig. 3.6 The principal difference of these configuration is in the ASE pattern and inversion profile.

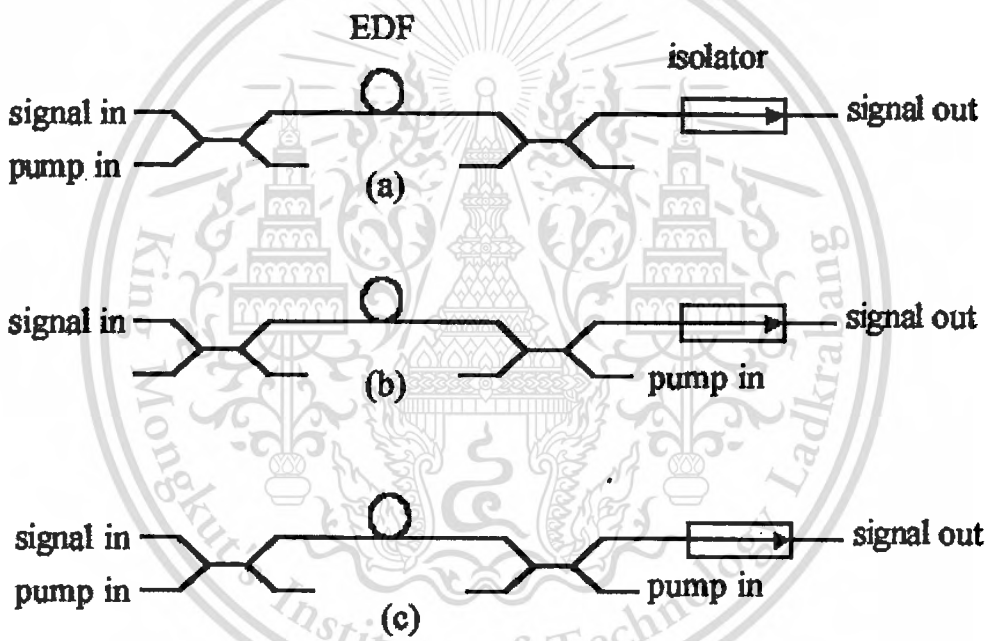

Fig. 3.6 EDFA pump configurations: (a) co-propagating pumping (b) counter-propagating pumping (c) bidirectional pumping.

Forward pumping displays better noise performance than backward pumping, while backward pumping has the advantages of higher saturation power and higher gain. Bidirectional pumping has the merits of both at the cost of complexity.

3.3.2 Fiber Length

The choice of the fiber length is determined by the efficiency and noise figure. A long fiber will absorb all the pump power resulting in the highest gain for a given pump power. A shorter fiber will let a significant portion of pump light to exit, but will on the other hand, be well inverted across the length thus offering a good noise figure .

3.3.3 Pump Sources

Typically, two types of pump sources are used in modern EDFAs : 980nm and 1480nm laser diodes. The choice of 1480nm pump yields a better power conversion efficiency, compared to 980nm light. However, the noise figure is smaller with 980nm pump since it can offer higher inversion population .

3.3.4 Multistage amplifiers

For a single-stage amplifier, the requirements of high gain and gain efficiency are often in conflict with the objective of a low noise figure. The key advantage of multistage amplifiers is that they allow elimination of a significant portion of ASE at the middle point of the amplifier. By reducing the ASE, more gain is available for the signal and less noise is added. Various forms of multistage amplifiers have been used in practice as shown in Fig. 3.7, however they all have the same feature of separating successive fiber sections by optical elements that reduce ASE in favour of signal. It is often advantageous to pump the first stage with 980nm light and the second stage with 1480nm light. The 980nm pump has the benefit of low noise figure at the all-important input portion, whereas 1480nm pumping offers a much higher optical conversion efficiency for the power amplifier port.

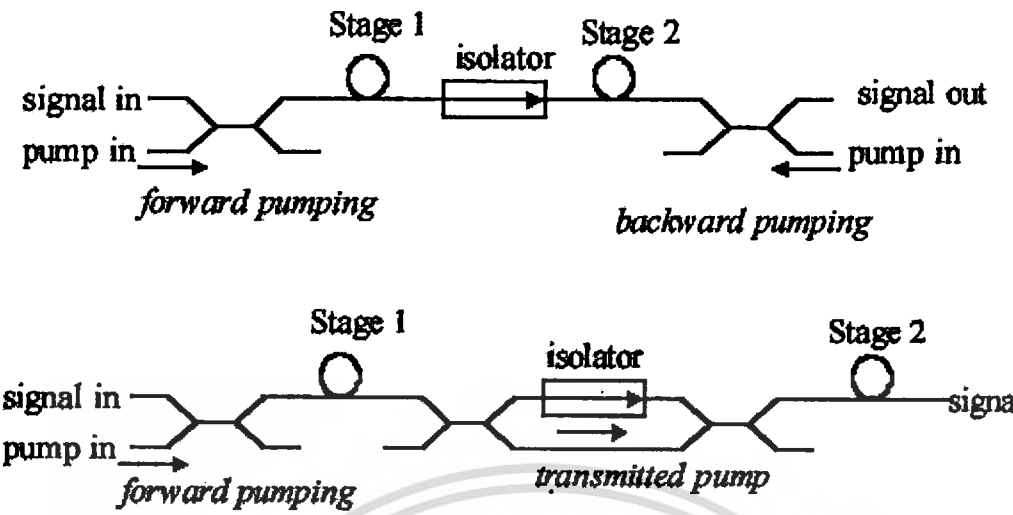

Fig 3.7 Configuration of the multistage amplifiers with various possible pump configurations .

3.4 Noise

Amplifier noise is unavoidable but can be reduced by using low pump powers. This fundamental property can be found using both semi-classical and quantum-mechanical approaches. The major manifestation of noise in the EDFA is in the form of amplified spontaneous emission (ASE) noise. Spontaneous emission is present in the spectral interval corresponding to the gain spectrum of the amplifier, and spectral density is proportional to the gain. The noise power at the signal wavelength is calculated from the expression

$$P_{ASE} = 2\, n_{sp}(G-1)hv\, B_o \tag{3.39}$$

where v is the signal frequency, h is Planck's constant, B_o is the bandwidth of the optical spectrum analyzer at the signal frequency v . n_{sp} is the inversion factor given by

$$n_{sp} = \frac{\sigma_e N_2}{\sigma_e N_2 - \sigma_a N_1} \tag{3.40}$$

where σ_e is emission cross-section, σ_s is the absorption cross-section, N_1 is the population of the first energy level and N_2 is the population of the second energy level. The noise figure (NF)

of the EDFA is commonly used as a measure of the degradation of the signal-to-noise ratio for signal passing through the amplifier ($NF = SNR_{in} / SNR_{out}$). in out The expression to calculate the optical noise figure is given by.

$$NF(dB) = 10\log_{10}\left(\frac{P_{ASE}}{h\nu B_o} + \frac{1}{G}\right) \tag{3.41}$$

Eq. (3.41) assumes that no noise is injected at the input of the amplifier (i.e., a shot-noise-limited input signal).

CHAPTER 4

PULSE PROPAGATION AND NONLINEAR IN OPTICAL FIBER

For an understanding of the nonlinear phenomena in optical fibers, it is necessary to consider the theory of electromagnetic wave propagation in dispersive nonlinear media. The objective of this chapter is to obtain discuss fiber characteristics, fiber nonlinearities and grove velocity dispersion and basic equation that governs propagation of optical pulses in single mode fibers. We discuss nonlinear in optical fiber ring resonator such as kerr effect and four-wave mixing(FWM), we consider the origin of FWM and discuss its theory. Nonlinear fiber optics has continued to grow during the decade of 1990s, perhaps even more dramatically than anticipated. This growth is motivated by several recent advances in lightwave technology, the most important being the advent of high-capacity fiber-optic communication systems. In such systems, the transmitted signal is amplified periodically by using optical amplifiers to compensate for residual fiber losses. As a result, the nonlinear effects accumulate over long distances, and the effective interaction length can exceed thousands of kilometers! It is impossible to review the entire field of nonlinear fiber optics.

4.1 Fiber Characteristics

Before describing the nonlinear effects in optical fibers, it is worthwhile to ponder why optical fibers are useful for nonlinear optics. This section describes the properties of optical fibers that are unique to them and their relevance to the study of nonlinear optical phenomena.

4.1.1 Single-Mode Fibers

An optical fiber looks like a thin strand of glass and consists of a central core surrounded by a cladding whose refractive index is slightly lower than that of the core. Both the core and the cladding are made of fused silica, a glassy material with an ultra-low loss (about 0.2 dB/km) in the near infrared region near 1.5 μm. The refractive-index difference between the core and the cladding is realized by the selective use of dopants during the fabrication process. Dopants such as GeO_2 and P_2O_5 increase the refractive index of pure silica and are suitable for the core, while

materials such as boron and fluorine are used for the cladding because they decrease the refractive index of silica. Even a relatively small refractive-index difference between the core and the cladding (typically less than 1%) can guide the light along the fiber length through the well-known phenomenon of total internal reflection. The guiding properties of an optical fiber are characterized by a dimensionless parameter defined as

$$V = a\left(\frac{\omega}{c}\right)\left(n_1^2 - n_2^2\right)^{1/2} \tag{4.1}$$

where a is the core radius, ω is the frequency of light, and n_1 and n_2 are the refractive indices of the core and the cladding, respectively. The parameter V determines the number of mode supported by the fiber. Optical fibers with $V < 2.405$ support only a single mode and are called single-mode fibers. Such fibers have a microscopic core ($a < 5$ μm) and are used almost exclusively for a variety of applications including optical communications.

4.1.2 Fiber Nonlinearities

The response of any dielectric to light becomes nonlinear for intense electromagnetic fields. In the transparent region of optical fibers, the lowest-order nonlinear effects originate from the third-order susceptibility $\chi^{(3)}$, which is responsible for phenomena such as third-harmonic generation, four-wave mixing (FWM), and nonlinear refraction. Among these, nonlinear refraction, a phenomenon referring to the intensity dependence of the refractive index, plays the most important role. The effective refractive index of the fiber mode has a general form

$$\tilde{n}(\omega I) = n(\omega) + n_2 I \tag{4.2}$$

where $n(\omega)$ is the linear part of the mode index at the frequency ω, I is the optical intensity, and n_2 is the nonlinear parameter related to $\chi^{(3)}$. Several physical mechanisms contribute to n_2, the dominant contribution coming from the anharmonic motion of valence electrons. Because of a fast response of such electrons, the frequency dependence of n_2 can often be ignored.

The intensity dependence of the refractive index leads to a large number of interesting nonlinear effects; the two most widely studied are self-phase modulation (SPM) and cross-phase modulation (XPM). SPM refers to the self-induced phase shift experienced by an optical field

during its propagation inside optical fibers. Its magnitude can be obtained by noting that the phase of an optical field changes during transmission through the fiber by

$$\phi = (n + n_2 I)k_0 L \tag{4.3}$$

where $k_0 = \omega/c = 2\pi/\lambda$, is the wavelength, and L is the fiber length.

The nonlinear phase shift resulting from SPM is $\phi_{NL} = n_2 k_0 L I$. Silica glass is a relatively weak nonlinear medium with a measured value of $n_2 \approx 2.7 \times 10^{-20}$ m^2/W. For silica fibers this value can vary in the range $n_2 = 2.2\text{-}3.0 \times 10^{-20}$ m^2/W depending on the density of dopants and on whether the fiber preserves polarization of light. However, even though n_2 is relatively small compared with most other nonlinear media, the nonlinear phase shift ϕ_{NL} can become large since the intensity I is enhanced in optical fibers by orders of magnitude because of a small mode diameter (typically < 10 μm). At the same time, relatively low losses in fibers can maintain this intensity over long lengths (~10 km). If fiber losses are compensated periodically by using optical amplifiers, the interaction length L can exceed thousands of kilometers. It is this combination of a high intensity and a long interaction length that makes optical fibers so attractive for nonlinear optics.

4.1.3 Group-Velocity Dispersion

As seen in Eq. (4.2), the refractive index in fibers also depends on the optical frequency. This chromatic dispersion plays an important role in nonlinear fiber optics under certain conditions. To understand its significance, consider a single-mode fiber of length L. A specific spectral component at the frequency would arrive at the output end of the fiber after a time delay $T = L/v_g$, where v_g is the group velocity defined as $v_g = (d\beta/d\omega)^{-1}$ and $\beta = n(\omega)\omega/c$ is the propagation constant.

The frequency dependence of the group velocity leads to pulse broadening simply because different spectral components of the pulse do not arrive simultaneously at the fiber output. If $\Delta\omega$ is the spectral width of the pulse, the extent of pulse broadening is governed by

$$\Delta T = \frac{dT}{d\omega}\Delta\omega = \frac{d}{d\omega}\left(\frac{L}{v_g}\right)\Delta\omega = L\frac{d^2\beta}{d\omega^2}\Delta\omega \equiv L\beta_2\Delta\omega \tag{4.4}$$

This phenomenon is referred to as the group-velocity dispersion (GVD), and the parameter $\beta_2 = d^2\beta/d\omega^2$ is known as the GVD parameter. In standard silica fibers, β_2 changes sign from positive to negative as wavelength of light increases beyond 1.3 μm. The region in which β_2 is negative is referred to as the anomalous-GVD regime. The magnitude of β_2 can be controlled by shifting the wavelength at which β_2 changes sign. Dispersion-shifted fibers used for optical communications are designed to have $\beta_2 = 0$ near 1.5 μm. It is possible to design fibers such that β_2 is relatively small over a wide wavelength range extending from 1.3 to 1.6 μm. Such fibers are called dispersion-flattened fibers. Recently, attempts have been made to produce fibers whose GVD decreases along the fiber length through axial variations in the core radius. Such fibers are called dispersion decreasing fibers and are likely to become important in near future.

4.2 Pulse-Propagation

The study of most nonlinear effects in optical fibers involves the use of short pulses with widths ranging from ~10ns to 10 fs. When such optical pulses propagate inside a fiber, both dispersive and nonlinear effects influence their shape and spectrum. In this section we derive a basic equation that governs propagation of optical pulses in nonlinear dispersive fibers. The starting point is the wave equation, it can be written in the form.

$$\nabla^2 \mathrm{E} - \frac{1}{c^2}\frac{\partial^2 \mathrm{E}}{\partial t^2} = \mu_0 \frac{\partial^2 \mathrm{P}_L}{\partial t^2} + \mu_0 \frac{\partial^2 P_{NL}}{\partial t^2} \tag{4.5}$$

Where the linear and nonlinear parts of the induced polarization are related to the electric field $\mathbf{E}(r, t)$.

4.2.1 Nonlinear Pulse Propagation

It is necessary to make several simplifying assumptions before solving Eq. 4.5. Fist, P_{NL} is treated as a small perturbation to P_L .This is justified because nonlinear changes in the refractive index are $< 10^{-6}$ in practice. Second, the optical field is assumed to maintain its polarization along the fiber length so that a scalar approach is valid. This is not really the case, unless polarization-maintaining fibers are used, but the approximation works quite Well in practice; it will be relaxed later. Third the optical field is assumed to be quasi-monochromatic, i.e., the pulse spectrum, centered at ω_0 ,is assumed to have a spectral width $\Delta\omega$ such that

$\Delta\omega/\omega_0 << 1$. Since $\omega_0 \sim 10^{15}\ s^{-1}$, the last assumption is valid for pulses as short as 0.1ps. In the slowly varying envelope approximation adopted here, it is useful to separate the rapidly varying part of the electric field by writing it in the form

$$E(r,t) = \frac{1}{2}\hat{x}\left[E(r,t)\exp(-i\omega_0 t) + c.c.\right] \tag{4.6}$$

Where $\hat{x}$ is the polarization unit vector, and E(r, t) is a slowly varying function of time (relative to the optical period).The polarization components P_L and P_{NL} can also be expressed in a similar way by writing

$$P_L(r,t) = \frac{1}{2}\hat{x}\left[P_L(r,t)\exp(-i\omega_0 t) + c.c.\right] \tag{4.7}$$

$$P_{NL}(r,t) = \frac{1}{2}\hat{x}\left[P_{NL}(r,t)\exp(-i\omega_0 t) + c.c.\right] \tag{4.8}$$

The general equation that describes the optical field evolution in a dielectric medium is given by

$$\nabla^2 E - \frac{1}{c^2}\frac{\partial^2 E}{\partial t^2} = -\mu_0 \frac{\partial^2 P(E)}{\partial t^2} \tag{4.9}$$

where the polarization P characterizes the medium and it is a function of the electrical field. In the case of weak nonlinear behavior of the medium, the polarization can be expressed by a Taylor polynomial as

$$P \approx \varepsilon_0\left\{\chi^{(1)}E + \chi^{(2)} : EE + \chi^{(3)} : EEE\right\} \tag{4.10}$$

where $\chi^{(1)}$ is the linear susceptibility, :represents the inner tensor product and the second and the third-order tensor $\chi^{(2)}$ and $\chi^{(3)}$ are responsible for the second harmonic generation, and the third-order harmonic generation, respectively. In optical fiber the term $\chi^{(2)}$ can be neglected, since it is different for zero only for medium without inversion symmetry at the molecular level; this is not the case of the fiber that is composed by symmetric molecules (SiO_2). As a consequence the nonlinear behavior of the fiber is mainly due to the $\chi^{(3)}$ term of the susceptibility. In particular, the real part for the Raman effect. Due to the presence of a coherent acoustic wave, the Brillouin scattering is very difficult to incorporate into an expression of $\chi^{(3)}$.

To analyze Simulated Brillouin Scattering (SBS), the coupled equation system composed by Eq. (4.10).

4.2.2 Nonlinear Schrodinger Equation

Most nonlinear effects in optical fibers are observed by using short optical pulses because the dispersive effects are enhanced for such pulses. Propagation of optical pulses through fibers can be studied by solving Maxwell's equations. In the slowly varying envelope approximation, these equations lead to the following nonlinear Schrodinger equation (NSE) .

$$\frac{\partial A}{\partial z}+\frac{i}{2}\beta_2\frac{\partial^2 A}{\partial t^2}=i\gamma|A|^2A-\frac{\alpha}{2}A \tag{4.11}$$

where A(z,t) is the slowly varying envelope associated with the optical pulse, α accounts for fiber losses, β_2 governs the GVD effects, and γ is the nonlinear parameter defined as

$$\gamma=n_2\omega/(cA_{eff}) \tag{4.12}$$

Here A_{eff} is the effective core area of the fiber. This equation is appropriate for pulses wider than 5 ps. For an accurate description of shorter pulses, several higher-order dispersive and nonlinear terms must be added to the NSE .

4.2.3 Modulation Instability

The nonlinear phenomenon of modulation instability is perhaps the simplest to understand since it follows readily from the NSE and emphasizes the role played by the GVD. Consider propagation of a continuous-wave (CW) beam of input power P_0 inside an optical fiber. If the fiber loss is ignored by setting α = 0, Eq. (4.11) is easily solved to yield $A_s(z)=\sqrt{P_0}\exp(i\phi_{NL})$, where $\phi_{NL}=\gamma P_0 z$ is the SPM-induced nonlinear phase shift. Eq. (4.11) thus shows that a CW beam should propagate through the fiber unchanged except for acquiring a power-dependent phase shift.

Before reaching this conclusion, however, one must ask whether the steady-state solution $A_s(z)$ is stable against small perturbations. To answer this question, to perturb the steady state

slightly such that $A(z,t)=\left[\sqrt{P_0}+a(z,t)\right]\exp(i\phi_{NL})$ and liberalize Eq. (4.11) in a(z,t) by assuming that the perturbation is relatively small. The resulting equation,

$$\frac{\partial a}{\partial z}+\frac{i}{2}\beta_2\frac{\partial^2 a}{\partial t^2}=i\gamma P_0\left(a+a^*\right) \tag{4.13}$$

is readily solved by assuming a general solution of the form

$$a(z,t)=a_1\cos(Kz-\Omega t)+ia_2\sin(Kz-\Omega t) \tag{4.14}$$

where Ω is the perturbation frequency and K is the wave number associated with it. By using Eqs. (4.13) and (4.14), K is found to be given by

$$K(\Omega)=\pm\frac{1}{2}|\beta_2|\Omega\left[\Omega^2+(4\gamma P_0/\beta_2)\right]^{1/2} \tag{4.15}$$

The dispersion relation Eq. (4.15) shows that stability of the CW solution depends critically on whether light experiences normal or anomalous GVD inside the fiber. In the case of normal GVD ($\beta_2 > 0$), the wave number K is real for all Ω, and the CW beam is stable against small perturbations. By contrast, in the case of anomalous GVD ($\beta_2 < 0$), K becomes imaginary for a range of frequencies, and the perturbation a(z,t) grows exponentially with z. Thus, propagation of CW beams through fibers is inherently unstable when $\beta_2 < 0$. This instability is referred to as the modulation instability since it leads to spontaneous modulation of the CW beam at a certain frequency whose value depends on the beam power. Similar instabilities occur in many other nonlinear systems and are often called self-pulsing instabilities.

4.3 Optical Kerr Effect

Nonlinear effect in optical fibers is due either to changes in the refractive index with optical power or to scattering phenomenal. The power dependence of refractive index is responsible for the Kerr effect. Depending on the shape of the input signal, the Kerr nonlinearity manifests itself by different effect, such as self-phase modulation, cross-phase modulation, Nonlinear behaviors of light traveling in fiber optic are commonly induced by the effects such as Kerr effects, four-wave mixing, and the external nonlinear pumping power. The device

characteristics that suit to implement in the practical communication system has seen. To meet the practical applications, the micro ring and Add/drop parameters are needed to make them satisfy the usual fabrication. The analogy of chaotic signal generation using fiber ring resonator and the related behaviors are described.

The presence of $\chi^{(3)}$ implies that the refractive index depends on the field intensity, I, in the form

$$n = \sqrt{1 + \chi^{(1)} + \frac{3}{2}\frac{\chi^{(3)}}{c\varepsilon_0 n_0} I} \approx n_0 + n_2 I \tag{4.16}$$

where $n_0 = \sqrt{1+\chi^{(1)}}$ and $n_2 = 3\chi^{(3)}/(4c\varepsilon_0 n_0^2)$. In Eq. (4.16), n_0 is the linear refractive index, whereas n_2 is the refractive index nonlinear coefficient, also known as the Kerr coefficient.

In the case of silica fibers, we have $n_0 \approx 1.46$ and $n_2 \approx 3.2\times10^{-20} m^2/W$. Considering a single-mode fiber with an effective mode area $A_{eff} = 50\mu m^2$ carrying a power P = 100 mW, the nonlinear part of the refractive index is

$$n_2 I = n_2 \frac{P}{A_{eff}} \approx 6.4\times10^{-11} \tag{4.17}$$

In spite of this very small value, the effects of the nonlinear component of the refractive index become significant due to very long interaction lengths (10 – 10,000 km) provided by the optical fibers. The Kerr nonlinearity gives rise to different effects, depending on the shape of the field injected into the fiber. In the following, the main effects due to Kerr nonlinearity will be reviewed.

4.4 Four Wave Mixing

4.4.1 Origin of Four-Wave Mixing

The nonlinear response of bound electrons of a material to an applied optical field. More specifically, the polarization induced in the medium is not linear in the applied field but contains nonlinear terms whose magnitude is governed by the nonlinear susceptibilities. The parametric processes can be classified as second or third order processes depending on

whether the second-order susceptibility $\chi^{(2)}$or the third-order susceptibility $\chi^{(3)}$ is responsible for them. The second-order susceptibility $\chi^{(2)}$ vanishes for an isotropic medium in the dipole approximation. For this reason, the second-order parametric processes, such as second-harmonic generation and sum-frequency generation, should not occur in silica fibers. In practice, these processes do occur because of quadruple and magnetic-dipole effects, but with a relatively low conversion efficiency. Unexpectedly high conversion efficiencies (~1%) for second-harmonic generation have been observed in optical fibers under specific conditions.

The third-order parametric processes involve, in general, nonlinear inter action among four optical waves and include the phenomena such as third-harmonic generation, FWM, and parametric amplification. FWM in optical fiber has been studied extensively because it can be quite efficient for generating new waves . Its main features can be understood by considering the third-order polarization term given as

$$P_{NL} = \varepsilon_0 \chi^{(3)} : EEE, \tag{4.18}$$

Where E in the electric field, P_{NL} is the induced nonlinear polarization, ε_0 and is the vacuum permittivity.

Consider four optical waves oscillating at frequencies ω_1, ω_2, ω_3, and ω_4 linearly polarized along the same axis x. The total electric field can be written as

$$E = \frac{1}{2}\hat{x}\sum_{j=1}^{4} E_j \exp[i(k_j z - \omega_j t)] + c.c., \tag{4.19}$$

Where the propagation constant $k_j = n_j /c$, n_j is the refractive index, and all four waves are assumed to be propagating in the same direction. If we substitute Eq. (4.19) in Eq. (4.18) and express P_{NL} in the same form as E using

$$P_{NL} = \frac{1}{2}\hat{x}\sum_{j=1}^{4} P_j \exp[i(k_j z - \omega_j t)] + c.c., \tag{4.20}$$

We find that P_j (j = 1 to 4) consists of a large number of terms involving the products of three electric fields. For example, p_4 can be expressed as

$$P_4 = \frac{3\varepsilon_0}{4}\chi^{(3)}_{XXXX}[|E_4|^2 E_4 + 2(|E_1|^2 + |E_2|^2 + |E_3|^2)E_4 + 2E_1E_2E_3\exp(i\theta_+) + 2E_1E_2E_3^*\exp(i\theta_-) + ...] \quad (4.21)$$

Where θ_+ and θ_- are defied as

$$\theta_+ = (k_1+k_2+k_3-k_4)z-(\omega_1+\omega_2+\omega_3-\omega_4)t, \quad (4.22)$$

$$\theta_- = (k_1+k_2-k_3-k_4)z-(\omega_1+\omega_2-\omega_3-\omega_4)t, \quad (4.23)$$

The first four terms containing E_4 in Eq. (4.21) are responsible for the SPM and XPM effects. The remaining terms result from FWM. How many of these are effective in producing a parametric coupling depends on the phase mismatch between E_4 and P_4 governed by θ_+,θ_-, or a similar quantity.

Significant FWM occurs only if the phase mismatch nearly vanishes. This requires matching of the frequencies as well as of the wave vectors. The latter requirement is often referred to as phase matching. In quantum-mechanical terms, FWM occurs when photos from one or more waves are annihilated and new photons are created at different frequencies such that the net energy and momentum are conserved during the parametric interaction. The main difference between the parametric processes and the stimulated scattering processes is that the phase-matching condition is automatically satisfied in the case of stimulated Raman or Brillion scattering as a result of the active participation of the nonlinear medium. By contrast, the phase-matching condition requires a specific choice of the frequencies and the refractive indices for parametric processes to occur.

There are two types of FWM terms in Eq. (4.21) The term containing θ_+ corresponds to the case in which three photons transfer their energy to a single photon at the frequency $\omega_4 = \omega_1+\omega_2+\omega_3$. This term is responsible for the phenomena such as third-harmonic generation ($\omega_1 = \omega_2 = \omega_3$), or frequency conversion when $\omega_1 = \omega_2 \neq \omega_3$. In general, it is difficult to satisfy the phase-matching condition for such processes to occur in optical fibers with high efficiencies. The term containing θ_- in Eq. (4.21) corresponds to the case in which two photons at frequencies ω_1 and ω_2 are annihilated with simultaneous creation of two photos at frequencies ω_3 and ω_4 such that

$$\omega_3 + \omega_4 = \omega_1 + \omega_2. \tag{4.24}$$

The phase-matching requirement for this process to occur is

$$\begin{aligned} \Delta k &= k_3 + k_4 - k_1 - k_2 \\ &= (n_3\omega_3 + n_4\omega_4 - n_1\omega_1 - n_2\omega_2)/c = 0. \end{aligned} \tag{4.25}$$

It is relatively easy to satisfy $\Delta k = 0$ in the specific case $\omega_1 = \omega_2$. This partially degenerate case is most relevant for optical fibers. Physically, it manifests in a way similar to SRS. A strong pump wave at ω_1 creates two sidebands located symmetrically at frequencies ω_3 and ω_4 with a frequency shift

$$\Omega_s = \omega_1 - \omega_3 = \omega_4 - \omega_1,$$

(4.26)

Where we assume for definiteness $\omega_3 < \omega_4$. The low-frequency sideband at and the high-frequency sideband at are referred to as the Stokes and anti-Stokes bands in direct analogy with SRS. The partially degenerate FWM was originally called three-wave mixing as only three distinct frequencies are involved in the nonlinear process . In this chapter, the term three-wave mixing is reserved for the processes mediated by $\chi^{(2)}$. The name four-photon mixing is also used for FWM synonymously. Note also that the Stokes and anti-Stokes bands are often called the signal and idler bands, borrowing the terminology from the field of microwaves, when an input signal at ω_3 is amplified through the process of FWM.

When the signal at difference frequencies propagates through the fiber, besides Cross-Phase Modulation (XPM), another important effect occurs: four-wave mixing

Four-wave mixing (FWM) is a parametric interaction among waves satisfying a given phase relationship called phase matching. Different phenomena may be originated by FWM process depending on the relation among interaction frequencies. If three optical fields with carrier frequencies ω_i $(i = 1, 2, 3)$ co propagates inside the fiber simultaneously, it appears

that the third-order polarization vector has several components: three components have the frequencies of the input fields, the others have an angular frequency ω_4 given by

$$\omega_4 = \omega_1 \pm \omega_2 \pm \omega_3 \tag{4.27}$$

If no field is present in the fiber at the frequency ω_4, a new field component is created at this frequency. If a field at the frequency ω_4 is already present in the fiber, it will be affected by the nonlinear interaction between the fields at ω_i, which causes crosstalk in multi-channel communication systems.

The phase-mismatch among all for waves is given by

$$\Delta\beta = \beta(\omega_1) + \beta(\omega_2) - \beta(\omega_3) - \beta(\omega_4) \tag{4.28}$$

where $\beta(\omega)$ is the propagation constant for an optical field with frequency ω. Assuming that the frequencies to be closely and equally spaced (i.e., $\omega_1 = \omega_2 - \Delta\omega$, $\omega_3 = \omega_2 - 2\Delta\omega$, $\omega_1 = \omega_2 - \Delta\omega$) and making a Taylor series expansion of all β s about the frequency ω_2, we get

$$\Delta\beta = 2\beta_2(\Delta\omega)^2 \tag{4.29}$$

where $\beta_2 = \partial^2\beta/\partial\omega^2$ is the group velocity dispersion (GVD). When $\beta_2 = 0$ we a perfect shave-phase matching and thus an efficient FWM. This situation is desirable for applications such as all-optical signal processing, wavelength conversion, pulse compression, etc[1,2]. FWM in optical fibers can also be used for generating spectrally inverted signal through the process of optical phase conjugation (OPC), which is useful for dispersion compensation. However, in WDM systems FWM causes a transfer of power from each channel to its neighbors. Such a power transfer not only results in the power loss for the channel but also induces inters channel crosstalk that degrades the system performance severely. This problem can be minimized using the technique of dispersion management, in which the fiber dispersion is kept locally high even though it is low on average. Non-zero dispersion shifted fibers have been developed with a finite but small dispersion (~2 to 8 ps/km-nm) in order to reduce FWM effects in actual fiber optic communication systems.

4.4.2 Theory of Four-Wave Mixing

Four-wave mixing transfers energy from a strong pump wave to two waves, upshifted and downshifted in frequency from the pump frequency ω_1 by an amount Ω_s given in Eq. (4.26) If only the pump wave is incident at the fiber, and the phase-matching condition is satisfied, the Stokes and anti-Stokes waves at the frequencies ω_3 and ω_4 can be generated from noise, similarly to the stimulated scattering processes. On the other hand, if a weak signal at ω_3 is also launched into the fiber together with the pump. The signal is amplified while a new wave at ω_4 is generated simultaneously. The gain responsible for such amplification is called the parametric gain. In this section, we consider the FWM mixing process in detail and drive an expression for the parametric gain. The nondegenerate case ($\omega_1 \neq \omega_2$) is considered for generality.

4.5 Erbium-doped fiber ring resonator

Consider the nonlinear fiber optic ring resonator incorporating an erbium-doped fiber configuration is depicted in Fig. 4.1, which is constructed by single ring resonator and 2x2 optical coupler. The circumference of the fiber ring is L.

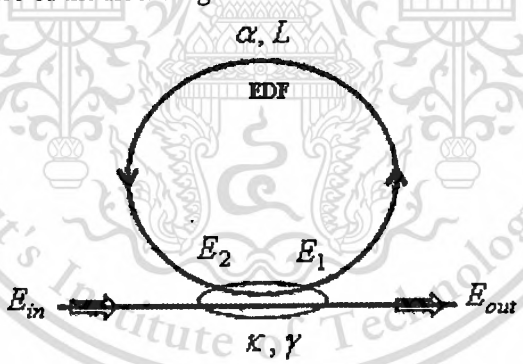

Fig. 4.1. Schematic of Erbium-doped fiber ring resonator

For convenience of analysis, we assume the complex electric field at each port as shown in Fig. 4.1. $E_{in}(t)$ is the incoming light field of an input port and the transmitted light field to the output port is $E_{out}(t)$. While the rest of the fields $E_1(t)$ and $E_2(t)$ are the circulated fields inside the fiber ring. Here, the input light is assumed to be monochromatic with constant amplitude and random phase modulation which results in temporal coherence degradation. Hence, the input light field can be expressed as

$$E_{in}(t) = E_0 \exp^{j\phi_0(t)} \tag{4.30}$$

According to light transmission theory in linear optical systems, we obtain the relations between the electric fields $E_1(t)$, $E_2(t)$, $E_{in}(t)$ and the output field $E_{out}(t)$ as following equations: η is the loss in the ring including the WDM insertion loss and splice losses between the EDF and the ordinary fiber ;

$$E_1(t) = \sqrt{1-\gamma}\left[\sqrt{1-\kappa}\,E_2(t) + j\sqrt{\kappa}\,E_{in}(t)\right]. \tag{4.31}$$

$$E_{out}(t) = \sqrt{1-\gamma}\left[\sqrt{1-\kappa}\,E_{in}(t) + j\sqrt{\kappa}\,E_2(t)\right]. \tag{4.32}$$

$$E_2(t) = \sqrt{G}\sqrt{1-\eta}\exp^{\frac{\alpha L}{2}j\phi}\,E_1(t). \tag{4.33}$$

and the total loss rate a is defined as

$$a = \sqrt{G(1-\gamma)(1-\eta)\exp^{\frac{\alpha L}{2}j\phi}} \tag{4.34}$$

G is the single-pass gain of Erbium-doped-fiber RR (EDFRR) for compensating the loss in the ring; and should be equal to or smaller than the single-pass loss l, namely.

$$G \le l = \frac{\exp^{\frac{\alpha L}{2}j\phi}}{(1-\gamma)(1-\eta)} \tag{4.35}$$

After one round-trip the electric field E_1 makes the nonlinearity inside the FORR is due to changes in the refractive index with optical power. Here, the power dependence of refractive index is responsible for the Kerr effect and the refractive index can be written as

$$n = n_0 + n_2 I = n_0 + (\frac{n_2}{A_{eff}})\left|E_1(t)\right|^2 \tag{4.36}$$

where n_0 and n_2 are the linear and nonlinear refractive indexes, respectively. I is the optical field intensity and the effective mode core area of the fiber is A_{eff}. Therefore, the circulated field E_2 has a phase shift including linear and nonlinear parts as

$$\phi = \phi_0 + \frac{\pi}{2} + \Delta\phi_{NL} \tag{4.37}$$

where $\phi_0 = kLn_0$ and $\phi_{NL} = kLn_2|E_1|^2$ are the linear and nonlinear phase shift, $k = 2\pi/\lambda$ is the wave propagation number in a vacuum. Substituting these parameters into Eq. (4.37) and then can be written as

$$\phi(t) = \phi_0 + \frac{\pi}{2} + \frac{2\pi n_2 L}{\lambda A_{eff}}|E_1(t)|^2 \tag{4.38}$$

CHAPTER 5

ENTANGLED PHOTONS

5.1 Quantum entanglement

Since quantum mechanics was born in the early 20th century, its controversial character has intrigued many physicists in their perception of nature. Undoubtedly, quantum mechanics offers a precise and elegant description of physical phenomena in various disciplines, ranging from subatomic physics to molecular physics and condensed-matter physics. In the shadow of this success, however, counterintuitive concepts of quantum mechanics have always been looming and have triggered several discussions on the foundations of quantum mechanics.

One of these concepts is quantum entanglement which originates from the well-known Gedanken experiment proposed by Albert Einstein, Boris Podolsky and Nathan Rosen (EPR) in 1935 [21]. In this experiment, two physical systems are considered to interact with respect to a certain observable. Due to the interaction the two systems will exhibit a strong mutual relation with respect to this observable. This so-called quantum entanglement means that the individual outcomes of the observables cannot be predicted with certainty for each of the two EPR systems, but the outcomes of the observables for the two systems are always strictly correlated. Quantum entanglement offends physical reality in the sense that the individual Measurement results are fundamentally undetermined before the measurement. According to quantum mechanics, a measurement of a certain value of the observable in one EPR system instantaneously determines the state of the other system, irrespective of the distance between the systems. This latter condition implies that quantum entanglement also contradicts the concept of locality. The EPR paper thus concluded that quantum mechanics is apparently incompatible with a local and realistic description of nature, and therefore cannot be considered as a "complete theory".

It was not until 1964 that John Bell translated the some what philosophical EPR discussion into a concrete test of the conflict between local realism and quantum mechanics [22]. This test consists of a set of inequalities which must be satisfied by any local and realistic theory. Quantum mechanics, however, predicts violation of these so-called Bells inequalities for measurements on specific quantum-entangled systems. Some years later, Clauser, Horne, Shimony and Holt (CHSH) introduced a generalized version of Bells inequalities which applies to

real laboratory experiments with, for example, quantum-entangled photons [23]. By now, many of such experiments on EPR particles have shown strong violation of Bells

Inequalities and thus confirmed the non-local nature of entanglement [24–26]. Especially in the last 15 years, investigations on the fundamental concept of quantum entanglement have also led to perspective applications in information science, such as quantum cryptography [27,28], quantum teleportation [29,30] and quantum computation [31].

5.2 Quantum Entangled photons

The first experimental proof of quantum entanglement via violation of Bell's inequalities was reported by Clauser and Shimony in 1978 [24]. A few years later, Aspect and co-workers [25] performed similar experiments in a more efficient way which yielded even more convincing results. For this pioneering work, photon pairs were used as the EPR particle systems. Ever since this major breakthrough, these photon pairs have remained the most popular tool for testing quantum correlations.

Despite the success of these early-generation EPR experiments[32], the employed atomic cascade source of photon pairs has only incidentally been employed in follow-up experiments because of the poor pair-production rate and collection efficiency. Instead, the production of quantum-entangled photons via the non-linear process of spontaneous parametric down-conversion (SPDC) in a bifringent crystal [33] became more favorable. In fact, the first SPDC source of photon pairs was already presented by Burnham and Weinberg in 1970 [34]. They successfully observed photon coincidences by matching the detection to the energy- and momentum-conservation conditions of the SPDC process. The new generation of EPR experiments [32], where a SPDC source is used to test the quantum correlations between photons, was simultaneously introduced by two groups in the late 80s [26], and quickly adopted by others [27]. The popularity of EPR photon pairs is also reflected by the ongoing development of high-quality and high-intensity SPDC sources [34,35].

As mentioned before, the entanglement of two-particle systems is always with respect to a certain observable. For quantum-entangled photons three of such observables can be distinguished, being polarization, energy or time (longitudinal space), and transverse momentum or transverse space. The corresponding types of entanglement are called polarization, time and spatial entanglement of photons, respectively. The entanglement of photons is in principle

simultaneous in the three mentioned observables. In this respect, one can also speak about multi parameter or hyper entanglement [36,37].

In the first entanglement experiments[24,25] only polarization correlations of EPR photons were measured. Since then, EPR experiments with polarization-entangled photons have always been most popular due to their practical simplicity [34,35]. Time entanglement of photons has been widely investigated in several interferometric schemes [37]. Somewhat less explored are the spatial correlations of entangled photons. The most notable experiments on spatial entanglement study these correlations by conditional imaging of the transverse positions of the pair-photons [38,39].

5.2.1 The biphoton wavefunction

Mathematically speaking, two particles1and2 are said to be entangled if their joint quantum state cannot be factorized into the quantum states of the individual particles. The physical interpretation of entanglement is that measurement of a quantum observable on particle 1 instantaneously determines the outcome of this observable for particle 2 and vice versa, irrespective of the inter particle distance and without any manipulation of particle 2. Two photons can be entangled in their polarization, transverse momentum or frequency, which implies that their two-photon wave function is non-factorizable in either of these degrees of freedom.

In general, the two-photon state produced via spontaneous parametric down conversion in a nonlinear crystal can be represented by the wave function .

$$|\psi\rangle = \int dq_1 \int dq_2 \int d\omega_1 \int d\omega_2 \sum_{i=H,V} \sum_{j=H,V} \Phi_{ij}(q_1,\omega_1;q_2,\omega_2)\hat{a}_i^+(q_1,\omega_1)\hat{a}_j^+(q_2,\omega_2)|0\rangle \quad (5.1)$$

The creation operators $\hat{a}_i^+(q_1,\omega_1)$ and $\hat{a}_j^+(q_2,\omega_2)$ act on the vacuum state $|0\rangle$, and create a photon in beam 1 with transverse momentum q_1 ,frequency ω_1 and polarization i, and a photon in beam 2 with transverse momentum q_2 ,frequency ω_2 and polarization j, respectively. The polarizations of photon 1 and 2 are labeled by indices i and j where the summation is over the horizontal (H) and vertical (V) polarization. Conservation of energy and transverse momentum in the down-conversion process requires $\omega_p = \omega_1 + \omega_2$ and $q_p = q_1 + q_2$.

The physics of the SPDC process and the quantum entanglement are contained in the biphoton amplitude functions $\Phi_{ij}(q_1,\omega_1;q_2,\omega_2)$. In fact, these amplitude functions depend on

three different aspects that embody(i) the transverse profile of the pump field E_p (q_p, ω_p), (ii) the phase mismatch built up during propagation inside the generating crystal and (iii)the two-photon propagation from the crystal plane to the detection plane.

5.2.2 The polarization-entangled photons

For the study of polarization entanglement, we consider two-photon production via type-II SPDC where the generated pair-photons have orthogonal polarizations, i.e., either i, j = H,V or i, j = V,H. The two-photon state in Eq. (5.1)can now be written as

$$|\psi\rangle = \int dq_1 \int dq_2 \int d\omega_1 \int d\omega_2 \{\Phi_{HV}(q_1,\omega_1;q_2,\omega_2)|H,q_1,\omega_1;V,q_2,\omega_2\rangle + \Phi_{VH}(q_1,\omega_1;q_2,\omega_2)|V,q_1,\omega_1;H,q_2,\omega_2\rangle\} \quad (5.2)$$

Physically speaking, the pair-photons are polarization entangled if one in principle cannot distinguish which photon (H or V) has travelled which path (1 or 2) on the basis of the measurement of any other variable than polarization. This is the case when the biphoton amplitude functions Φ_{HV} and Φ_{VH} overlap sufficiently well to prevent us to distinguish between the two states $|HV\rangle$ and $|VH\rangle$ on the basis of either frequency or spatial contents. The interference between these two probability channels is quantified by the wave function-overlap which is proportional to the coincidence count rate for simultaneous detection of one pair-photon in each detector.

An excited atom emits two photons that come out back to back from the Einstein Podolsky Rosen (EPR) source, with vanishing angular momentum and even parity. If $|x\rangle$ and $|y\rangle$ are horizontal and vertical linear polarization states of the photon, then have seen that

$$|+\rangle = \frac{1}{\sqrt{2}}(|x\rangle + i|y\rangle)$$

$$|-\rangle = \frac{1}{\sqrt{2}}(i|x\rangle + |y\rangle) \quad (5.3)$$

are the eigenstates of helicity. For two photons, one propagating light is in the $+\hat{z}$ direction and other in the $-\hat{z}$ direction. The states

$$|+\rangle_A|-\rangle_B$$
$$|-\rangle_A|+\rangle_B \qquad (5.4)$$

are invariant under rotations about $\hat{z}$. (The photons have opposite values of J_z, but the same helicity, since they are propagating in opposite directions.) Under a reflection in the y–z plane, the polarization states are modified according to

$$|x\rangle \to -|x\rangle \ , |+\rangle \to +i|-\rangle$$
$$|y\rangle \to |y\rangle \ , \ |-\rangle \to -i|+\rangle \qquad (5.5)$$

Therefore, the parity eigenstates are entangled states

$$\frac{1}{\sqrt{2}}\left(|+\rangle_A|-\rangle_B \pm |-\rangle_A|+\rangle_B\right) \qquad (5.6)$$

The state with $J_z = 0$ and even parity, then, expressed in terms of the linear polarization states, is

$$-\frac{i}{\sqrt{2}}\left(|+\rangle_A|-\rangle_B \pm |-\rangle_A|+\rangle_B\right) = \frac{1}{\sqrt{2}}\left(|xx\rangle_{AB} + |yy\rangle_{BA}\right)_n = |\phi^+\rangle_{AB} \qquad (5.7)$$

Because of invariance under rotations about $\hat{z}$, the state has this form irrespective of how we orient the x and y axes. We can use a polarization of either photon along any axis in the xy plane. Let $|x(\theta)\rangle$, and $|y(\theta)\rangle$ denote the linear polarization eigenstates along axes rotated by angle θ relative to the canonical x and y-axes. We may define an operator as (the analog of $\vec{\sigma}\cdot\hat{n}$)

$$\tau(\theta) = |x(\theta)\rangle\langle x(\theta)| - |y(\theta)\rangle\langle y(\theta)| \qquad (5.8)$$

Which has these polarization states as eigenstate with respective eigen values as

$$|x(\theta)\rangle = \begin{pmatrix} \cos\theta \\ \sin\theta \end{pmatrix},$$

$$|y(\theta)\rangle = \begin{pmatrix} -\sin\theta \\ \cos\theta \end{pmatrix} \tag{5.9}$$

Let $|H\rangle$ and $|V\rangle$ be two polarization states of photon, which are sent from Alice to Bob along two separated channels. We shall take two orthogonal states $|\psi_+\rangle$ and $|\psi_-\rangle$, linear combinations of $|H\rangle$ and $|V\rangle$ as show in Fig. 5.1 , to represent bit value "0" and bit value "1," respectively :

$$|\psi_+\rangle = \frac{1}{\sqrt{2}}(|H\rangle + |V\rangle) \tag{5.10}$$

$$|\psi_-\rangle = \frac{1}{\sqrt{2}}(|H\rangle - |V\rangle) \tag{5.11}$$

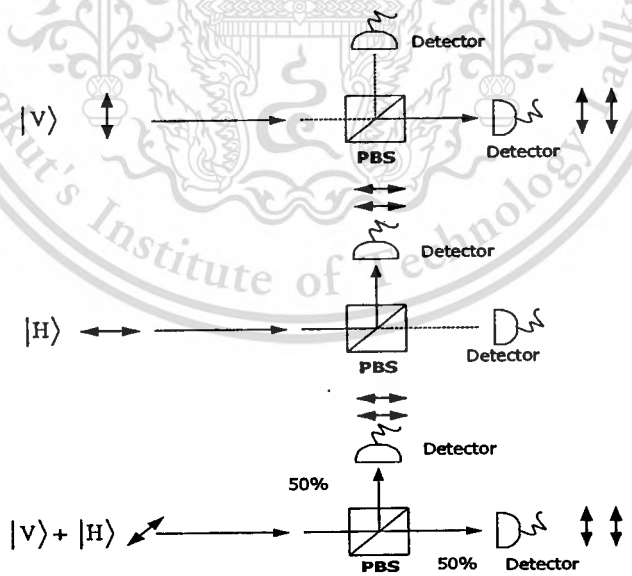

Fig. 5.1 Schematic diagram of a single photon entangled state.

Alice sends to Bob either $|\psi_+\rangle$ or $|\psi_-\rangle$. The two localized states, $|H\rangle$ and $|V\rangle$, are not sent together, but $|V\rangle$ is delayed for some time τ. For simplicity, we choose τ to be larger than the traveling time of the particles from Alice to Bob, θ. Thus $|V\rangle$ starts traveling towards Bob only when $|H\rangle$ already has reached Bob, such that the two wave packets and never found together in the transmission channels.

5.3 Entangled Photons Generation

A conventional fiber optic Mach-Zehnder interferometer is configured as an intrinsic sensor based on the interference between a sensing and a reference signal. A standard two-beam interferometer uses a laser diode as a coherent light source.

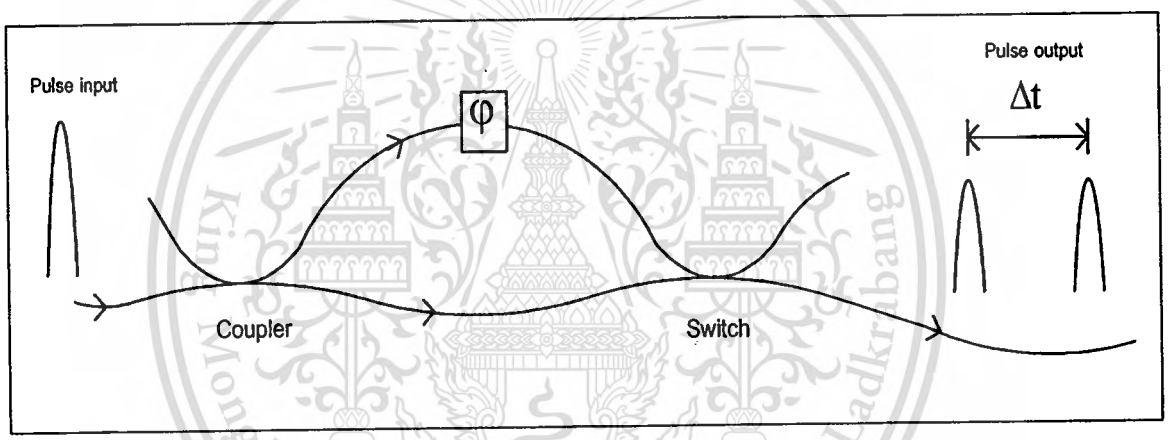

Fig. 5.2 A schematic of fiber optic Mach-Zhender interferometer.

To understand a system of all fiber optic interferometer, it is useful to start with the simple device, which can be entirely understood in terms of classical linear optics in Fig. 5.2 Let a 1-photon pulse enter into the device from left-hand side via one end of the coupler, which is assumed that it duration time is shot compared to the length difference of the interferometer arms. The incoming pulses were split by the first fiber-coupler between a short and a longer fiber path, in order to form a temporally separated pulse pair. The path lengths were chosen such that a relative time delay of 9.9 μs was obtained between the pair of pulses coupled into the transmission fiber via the second coupler. A phase shifter consisting of which could be varied by polarization control fiber (PC). The output pulses consists of two well-separated pulses which denote them shot and long respectively, which is presented the basis of quantum bit (qubit) space,

similarly to the usual vertical $|V\rangle$ and horizontal $|H\rangle$ linear polarization states. The relative norm and phase of the coefficients α and β are determined by the coupling ratio (η) of the coupler (beam splitter) and the phase φ of the phase shifter, respectively. Hence, any state of the two-dimensional Hilbert space spanned by the basic state can be prepared and analyzed. The duration time difference (Δt) of this Mach-Zehnder interferometer should be much longer than the pulse duration. The switch of the device recombines the pulse traveling through the short and the long arms without introducing any loss, which could be replaced by a passive fiber coupler. In our scheme, the photon wave function of one incident circular polarized photon will be split into two parts, transmitted part and the reflected part, by an ordinary nonpolarizing coupler. After interacting with the two parts of the photon wave function will be re-combined by the second ordinary nonpolarizing coupler. Through detecting the photon after the second coupler, we can decide whether the entangled photon pair has been created.

The correspondence between the polarization states and the states obtained by superposition of the two arm ones can be extended. For example, a polarization coupler that separates the basic vertical and horizontal polarization states corresponds to an optical switch between the short and the long pulses. We assume those horizontally polarized pulses with a temporal separation of Δt input into a Mach-Zehnder interferometer. The coherence time of the consecutive pulses is larger than Δt . Then the following time-bin entangled state is created through parametric in MZI.

$$|\Phi\rangle_p = |1,H\rangle_s |1,H\rangle_i + |2,H\rangle_s |2,H\rangle_i \tag{5.12}$$

In the expression $|k,H\rangle$, k is the number of time slots (1 or 2), where denotes the state of polarization [horizontal (H) or vertical (V)], and the subscript identifies whether the state is the signal (s) or the idler (i) state. In Eq. (5.12), for simplicity we have omitted an amplitude term that is common to all product states. We employ the same simplification in subsequent equations in this research. This two-photon state with H polarization shown by Fig. 5.2 is input into the orthogonal polarization-delay circuit shown schematically in Fig. 3.4. The delay circuit consists of a coupler and the difference between the round-trip times of the fiber ring resonator, which is equal to Δt . The polarization controller (PC) is tilted by changing the round trip of the fiber ring is converted into V at the delay circuit output. That is the delay circuits convert;

$$|k,H\rangle \text{ to } r|k,H\rangle + t_2\exp(i\phi)|k+1,V\rangle + \quad rt_2\exp(i_2\phi)|k+2,H\rangle + r_2t_2\exp(i_3\phi)|k+3,V\rangle$$

Where t and r is the amplitude transmittances to cross and bar ports in a coupler. Then Eq. (5.12) is converted into the polarized state by the delay circuit as

$$\begin{aligned}
|\Phi\rangle &= [|1,H\rangle_s + \exp(i\phi_s)|2,V\rangle_s] \\
&\times [|1,H\rangle_i + \exp(i\phi_i)|2,V\rangle_i] \\
&+ [|2,H\rangle_s + \exp(i\phi_s)|3,V\rangle_s] \\
&\times [|2,H\rangle_i + \exp(i\phi_i)|2,V\rangle_i] \\
&= [|1,H\rangle_s|1,H\rangle_i + \exp(i\phi_i)|1,H\rangle_s|2,V\rangle_i] \\
&+ \exp(i\phi_s)|2,V\rangle_s|1,H\rangle_i \\
&+ \exp[i(\phi_s+\phi_i)]|2,V\rangle_s|2,V\rangle_i \\
&+ |2,H\rangle_s|2,H\rangle_i + \exp(i\phi_i)|2,H\rangle_s|3,V\rangle_i \\
&+ \exp(i\phi_s)|3,V\rangle_s|2,H\rangle_i \\
&+ \exp[i(\phi_s+\phi_i)]|3,V\rangle_s|3,V\rangle_i
\end{aligned} \tag{5.13}$$

By the coincidence counts in the second time slot, we can extract the fourth and fifth terms. As a result, we can obtain the following polarization entangled state as

$$\begin{aligned}
|\Phi\rangle &= |2,H\rangle_s|2,H\rangle_i \\
&+ \exp[i(\phi_s+\phi_i)]|2,V\rangle_s|2,V\rangle_i
\end{aligned} \tag{5.14}$$

In this Fig. 5.3 the fiber acts as a nonlinear medium as a result of the optical Kerr effect. The use of long fiber with a small core is attractive for achieving a high optical intensity and long interaction length. The nonlinearity of the fiber is assumed to be of the Kerr type, i.e., the refractive index is given by

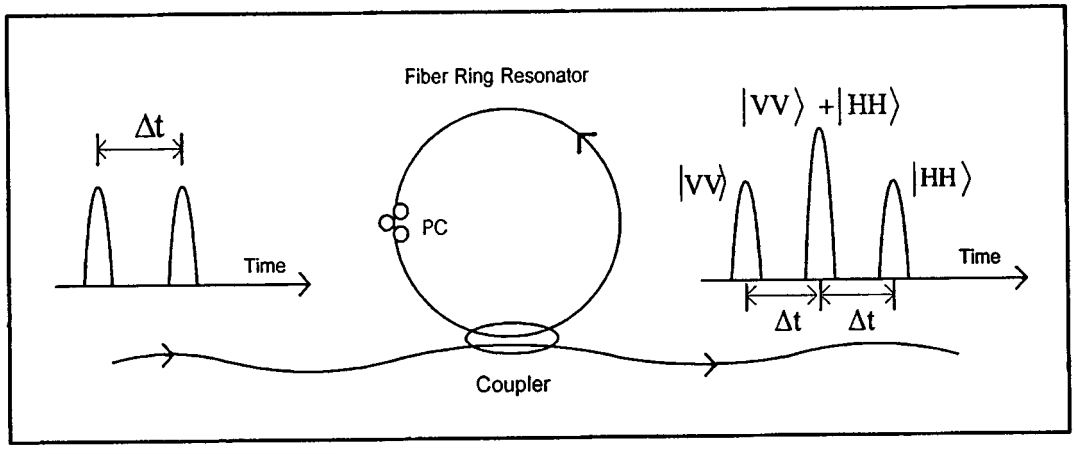

Fig. 5.3 A schematic diagram of the polarization delay circuit that uses in the experiment.

$$n = n_0 + n_2 I = n_0 + \frac{n_2 n_0}{2\eta_0}|E|^2$$
$$= n_0 + n_2 \frac{P}{S_{eff}} \qquad (5.15)$$

where n_0 and n_2 is the linear and nonlinear refractive index of the fiber respectively, and η_0 is the wave impedance in vacuum. I is the instantaneous optical intensity, E the optical electric field, and P the optical power. S_{eff} is the effective mode area depending on the modal field profile in the fiber. All numerical results presented here were calculated for the following values: linear index $n_0 = 1.45$, nonlinear index $n_2 = 3.0 \times 10^{-20}$ m^2 / W , and effective mode area $S_{eff} = 50$ μm^2. We assume that the response time of the Kerr effect is much less than the cavity round-trip time. Because of the Kerr nonlinearity of the optical fiber, the strong pulses acquire an intensity dependent phase shift during propagation. In the fiber ring resonator is arrangement, the weak and the strong propagating pulses acquire different nonlinear phase shifts. When the pulses interfere at the coupler, this relative phase shift realigns the axes of the ellipse. That the fiber optic MZI incorporating a nonlinear fiber optic ring resonator can be used to generate the pulsed polarization-entangled photon pairs, based on the conventional time-bin entanglement arrangement.

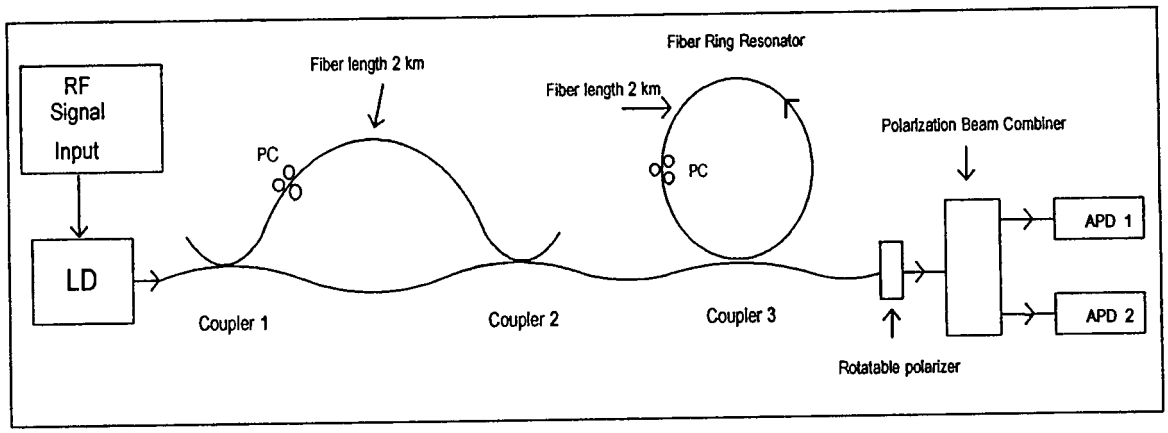

Fig. 5.4 The schematic of the experimental setup diagram; LD: Laser diode, PCs:Polarization Controllers, APD: Avalanche Photo detector.

In Fig. 5.4 Polarized light pulse is split in to two states via a fiber optic coupler, which randomly propagates in one of the interferometer arms. One of light beams propagates to polarization controller (PC 1) via a fiber optic with 2 km lengths, where the random combination of the entangled pulses is occurred at a second coupler (switch). The optical switch is separate the basic states without losses. The output photons consist of two well-separated pulse energy, which is entangled. Then the output pulses from MZI were launched into the nonlinear fiber ring resonator of the delay circuit. The delay circuit was made of 2-km fiber optic length. This fiber optic length can be designed to precisely adjust the required delay time i.e. Δt , while the change in phase being controlled by using the polarization controller (PC 2). The Kerr type nonlinearly of the effect of light pulses in the optical fiber is occurred while circulating in fiber ring resonator.

Since only the ratio of speed is involved in snell's law, only the ratio n is determine by measurements of refraction. The definition of the index of refraction of a single medium requires a convention. The convention used is that the index of refraction of a vacuum is exactly 1. Since the speed of light in vacuum is the constant c, the index of refraction n for a substance is given by

$$n = \frac{c}{v} \tag{5.16}$$

where v is the speed of light in the substance. It is important to note that without some definition of global time the physical quantity speed (and thus light-speed) has no definite meaning anyway. Consider an object moving from position A to B. Its speed v is given by the formula

$$v = \frac{S}{t} \tag{5.17}$$

where S is the distance of start to end of fiber optic, t is the time of the start and the finish time in fiber optic.

CHAPTER 6

EXPERIMENTS AND RESULTS

6.1 Experimental of Erbium-doped Fiber Laser.

Erbium-doped fiber laser(EDFL) can be constructed by the fiber ring cavity show in Fig. 6.1. We use the laser 980 nm for pump power in to the ring cavity via WDM coupler 2x1 and the two port of coupler are connected together to from a ring cavity containing the erbium-doped fiber. An isolator is inserted within the loop for unidirectional operation.

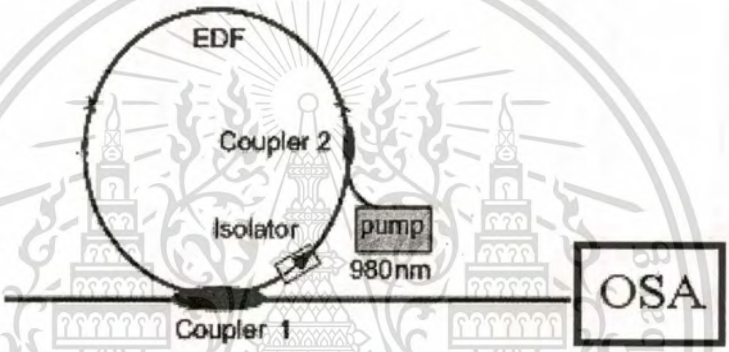

Fig. 6.1 Erbium-doped fiber laser schematic diagram.

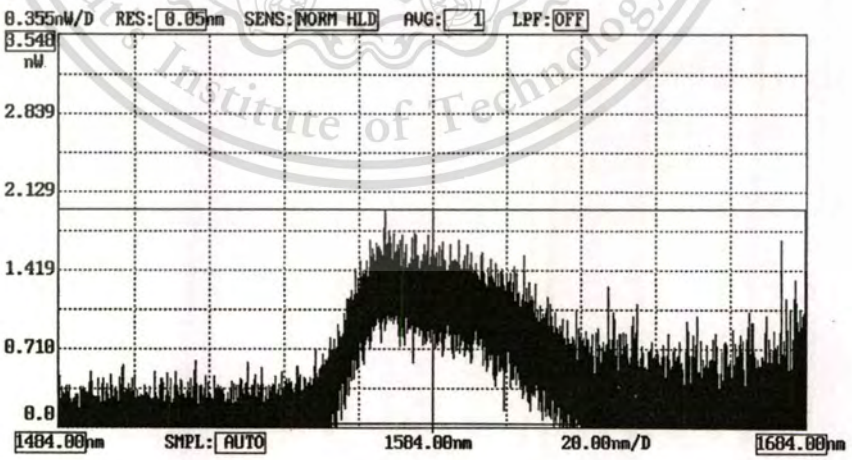

Fig. 6.2 The result of laser output Power versus wavelengths.

The result output power of fiber laser in this experiment are show in Fig.6.2. The spectra of the laser is obtained by the OSA at laser pump power 15 mW. The optical output power of spectrum peak at 1550 nm to 1600 nm. Amplified spontaneous emission(ASE) were propagate thought fiber ring cavity. This result have noise by ASE. In this experiment, I have constructed an Erbium-doped fiber amplifier and have investigated many of its important parameters, including the ASE spectrum, the pump threshold power, the emission cross-section, the conversion efficiency and the noise power dependency on pump power. Nonlinear optical loop mirrors in EDF ring resonator which induces intensity-dependent loss in a laser cavity and functions as an amplitude equalizer was employed to obtain stable multi wavelength oscillations in EDFL at room temperature.

6.2 Experimental of Entangled Photon States Re-generation.

6.2.1 Experiment setup.

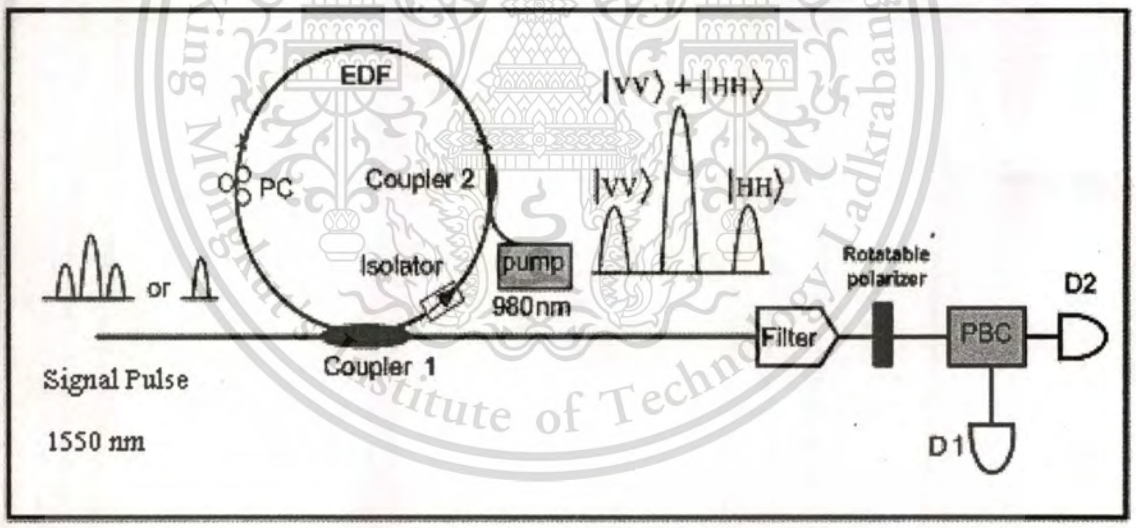

Fig. 6.3 A schematic diagram of the fiber optic ring resonator incorporating an erbium-doped fiber. PC: Polarization control, EDF: erbium-doped fiber, PBC: polarization beam combiner .

The experiment setup of the entangled photon states and amplitude recovery using a fiber ring resonator incorporating an erbium doped fiber(EDF) is shown in Fig. 6.3. The gain media is a length of high concentration EDF with peak absorption near 1530 nm of 5.0 - 8.0 dB/m, mode field diameter @ 1550 nm 4.9 - 6.3 μm. Fiber cladding has a diameter of 125 ± 1 μm, core-cladding concentricity < 0.3 μm, and numerical apertures are in the range of 0.21 - 0.25. A laser diode pump at 980 nm with maximum power 150 mW is connected to the EDF ring resonator via WDM coupler 1 and 2 with insertion loss is less than 0.3 dB. The optical tunable filter with large tuning range is employed to obtain the entangled photon states at the required wavelengths. The Erbium-doped fiber can be designed to obtain precisely the required amplified signals, while the change in phase is controlled by using the polarization controller (PC). The adjusting of the polarization angle from 0 to 90 degree, this can be performed by tilting the PC, which caused the change of both entangled states and optical output intensity. To confirm the existence of entangled states, then each photon was input into a polarizer and orientation from 0 to 180 degree before launching into the PBC. The output photons were detected by the avalanche photodiodes. The system consists a fiber ring resonator and pumping part (Erbium-doped fiber, EDF)with the certain polarization control states can produce the quantum entangled states i.e. quantum bits. They have shown that the random bits can be generated .

6.2.2 Experiment Results

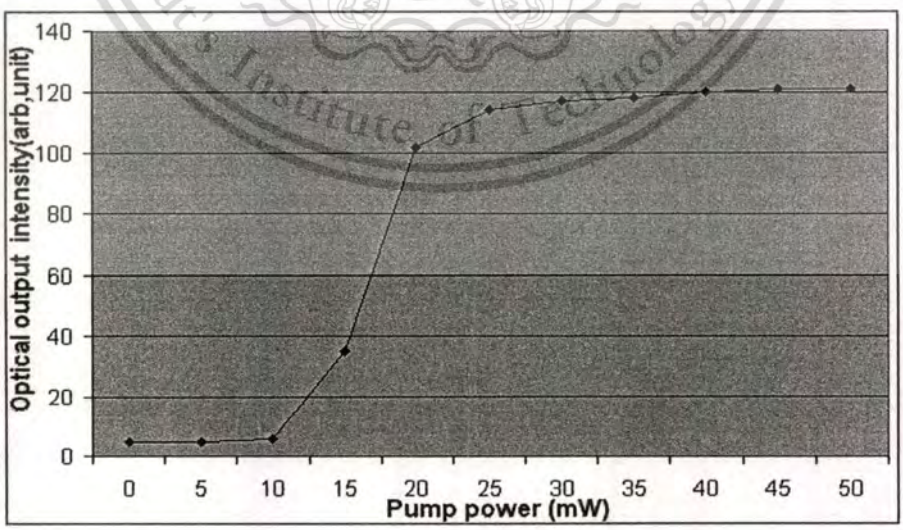

Fig. 6.4 Optical output intensity versus Pump power.

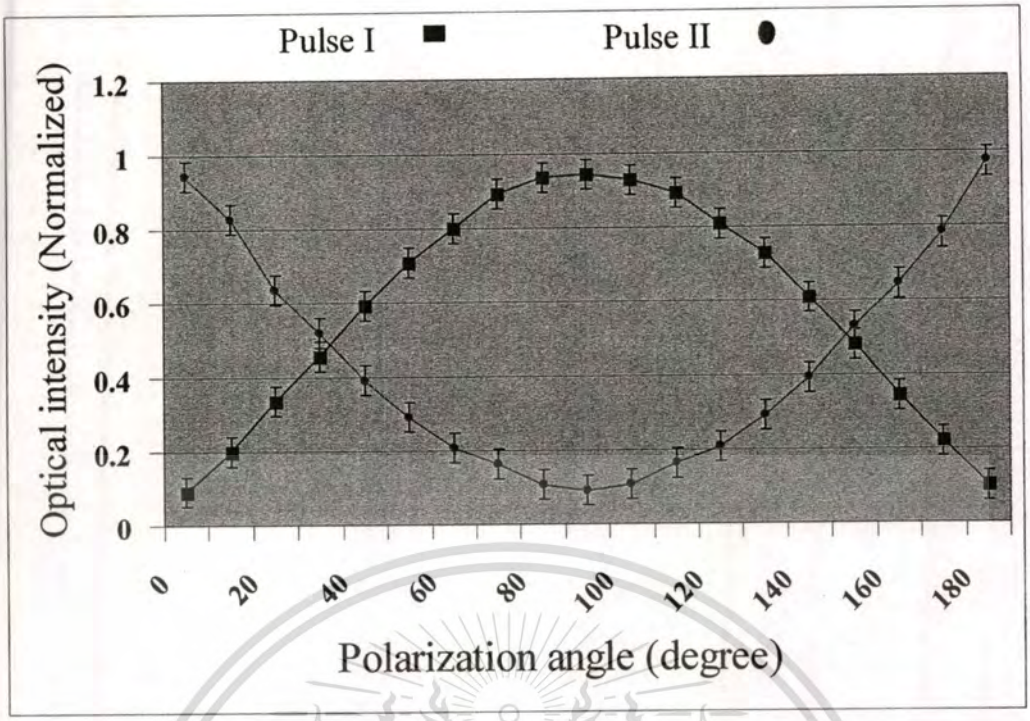

Fig. 6.5 (a) Optical intensity versus polarization angle (Pump power 0 mW).

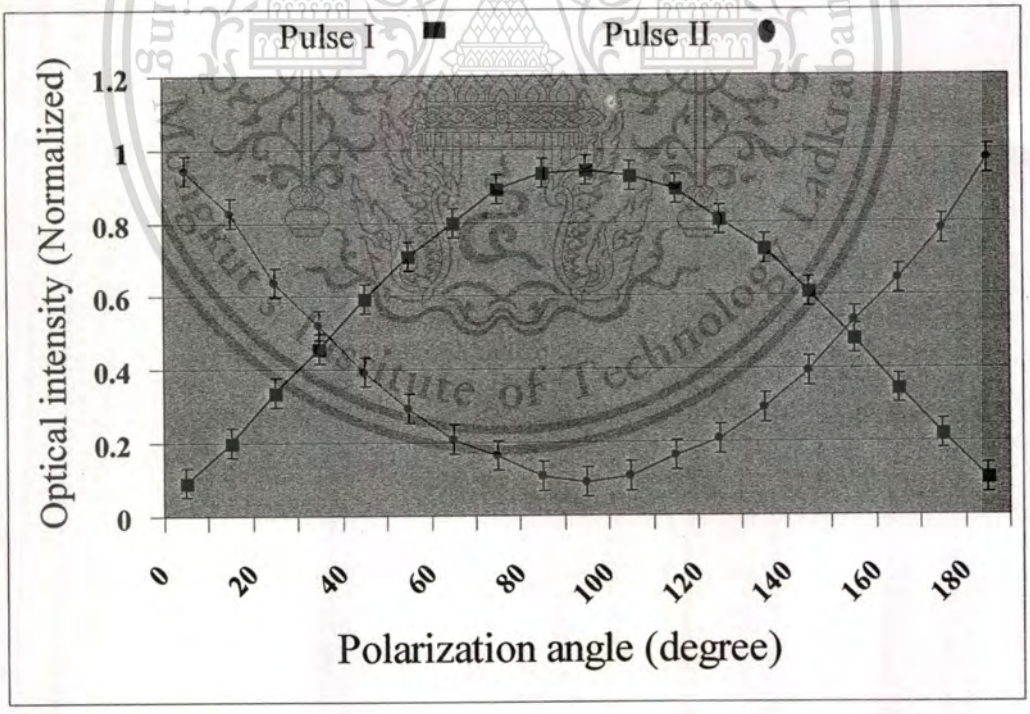

Fig. 6.5 (b) Optical intensity versus polarization angle (Pump power 10 mW).

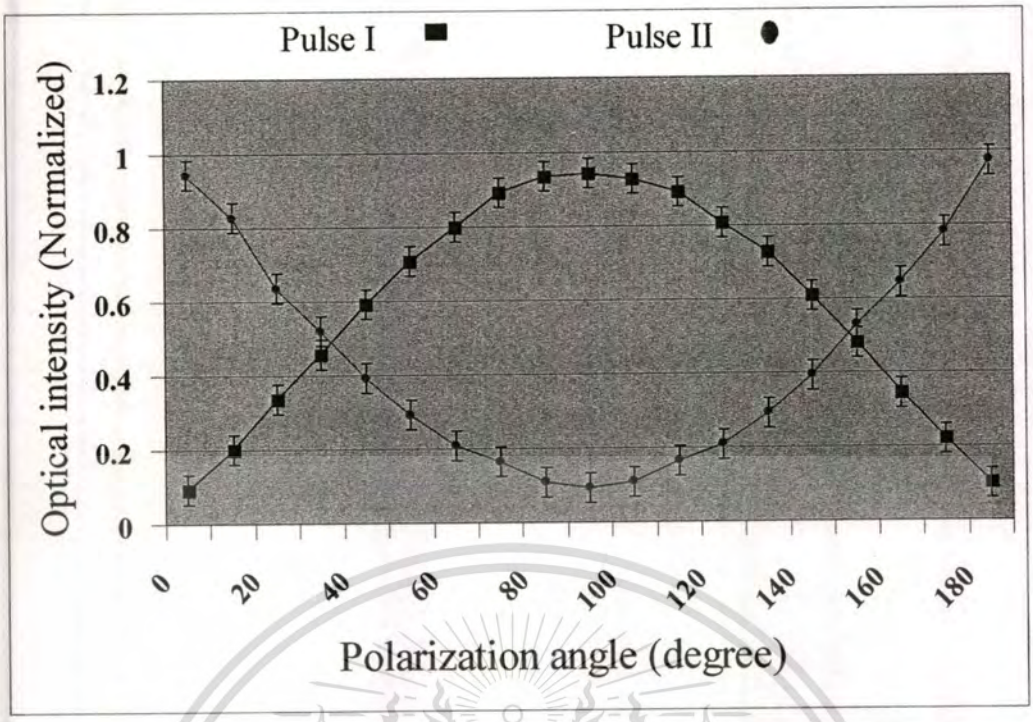

Fig. 6.5 (c) Optical intensity versus polarization angle (Pump power 20 mW).

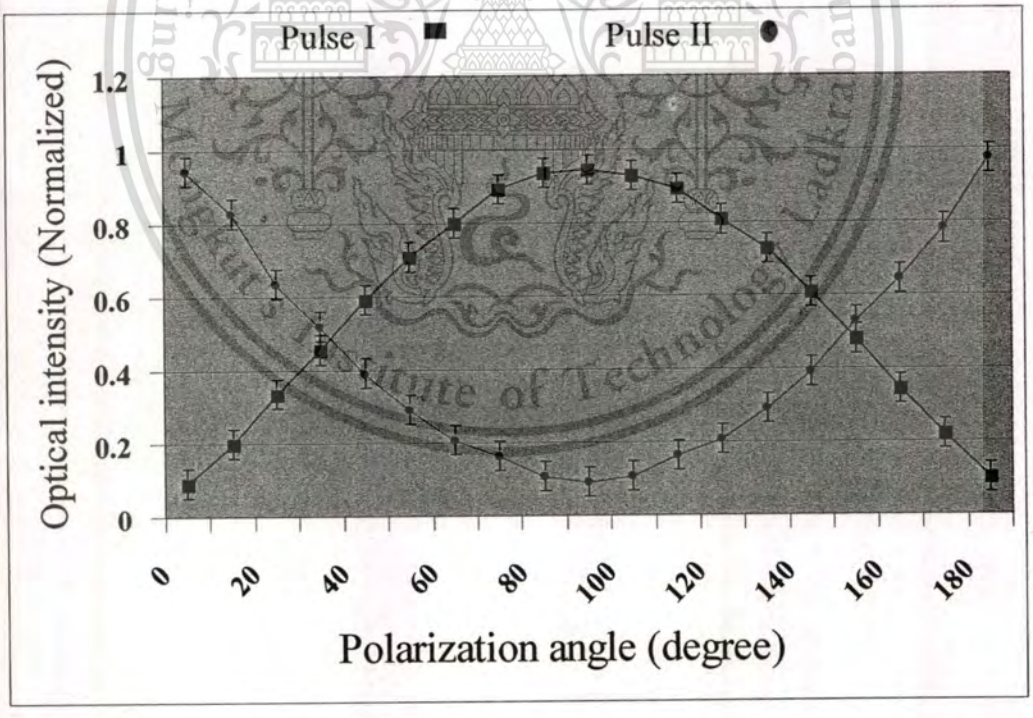

Fig. 6.5 (d) Optical intensity versus polarization angle (Pump power 30 mW).

The result output power show in Fig 6.4 , to measurement optical output intensity by varied laser pump power. This result have output intensity increate when pump power increate, saturation at pump power 40 mW and threshold pump power 10 mW.

The experimental results are shown in Fig. 6.5(a-d), where is a plot of the optical output intensity of the system Fig. 6.3 as a function of polarization angle when laser pump power 0 mW, 10 mW, 20 mW, 30 mW. This result shown polarization correlations each pump power not change , but output intensity increate when pump power increate. Thus the entangled photon regeneration by our system. Notice that the generated two-photon state is entangled with phase difference $\phi = 90^{\circ}$, which is detected by the avalanche photo detectors D1 and D2. The measurement errors of 4 % is shown by the error bar. The entangled photons due to the nonlinear effect in fiber optic ring resonator are specified by the signal and idler photons.

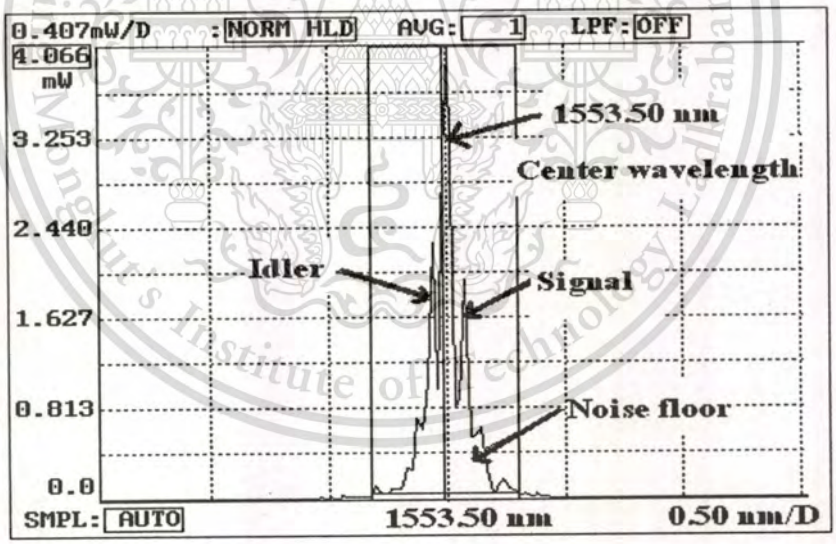

Fig. 6.6 Output spectrum.

Fig. 6.6 shows the output spectrum of the light pulse after circulating in the fiber ring resonator incorporation the EDF. Results obtained have shown that the signal gain up to 16 dB could be achieved, and the polarization entangled states recovered. We found that the noisy

signals occurred on the detected spectrum, due to the Kerr effect nonlinear type which is low power and amplified, become the noise floor of the experimental results. The ring-cavity lifetime is much longer than the Kerr-effect response time of the fiber ring. The transmission curves of the bistability and the instability are characterized subjecting to the coupler insertion losses (γ) and the coupling coefficients (K).However, the detected output still can be performed the entangled photon visibility and valid. In our device, the EDF is pumped by an LD at 980 nm to amplify the signal light at 1550 m. Now the principle of EDFA is well understood. The contributions of pump induced stimulated absorption and signal-induced stimulated emission and absorptions and spontaneous emission are only taken into account, and the difference between emission and absorption cross sections is neglected.

6.3 Experiment Thermal Effects of the Entangled Photon

6.3.1 Experimental Setup.

There are two experiments in this work, which one is the setup for the entangled photon generation and recovery, the other is the thermal effects investigation on the entangled photon and walk-off compensation. The experimental setup of the entangled photon states generation and re-generation with amplitude recovery part using a fiber ring resonator incorporating an EDFA is as shown in Fig 6.7. After the laser pulse with center wavelength of 1550 nm was launched into the system, the amplification part was employed. The gain media is consisted of a length of a high concentration EDF (15m), where the peak absorption at 1530 nm is ranged from 5.0 - 8.0 dB/m, and a mode field diameter at 1550 nm is ranged from 4.9 - 6.3 μm. A fiber cladding has a diameter of 125 ± 1 μm, core-cladding concentricity < 0.3 μm, and numerical apertures are in the range of 0.21 - 0.25. A laser diode pump at 980 nm with maximum power of 150 mW is connected to the EDF in a ring resonator via WDM couplers 1 and 2, which the insertion loss is less than 0.3 dB. The ring fiber radius used is 27 meters.

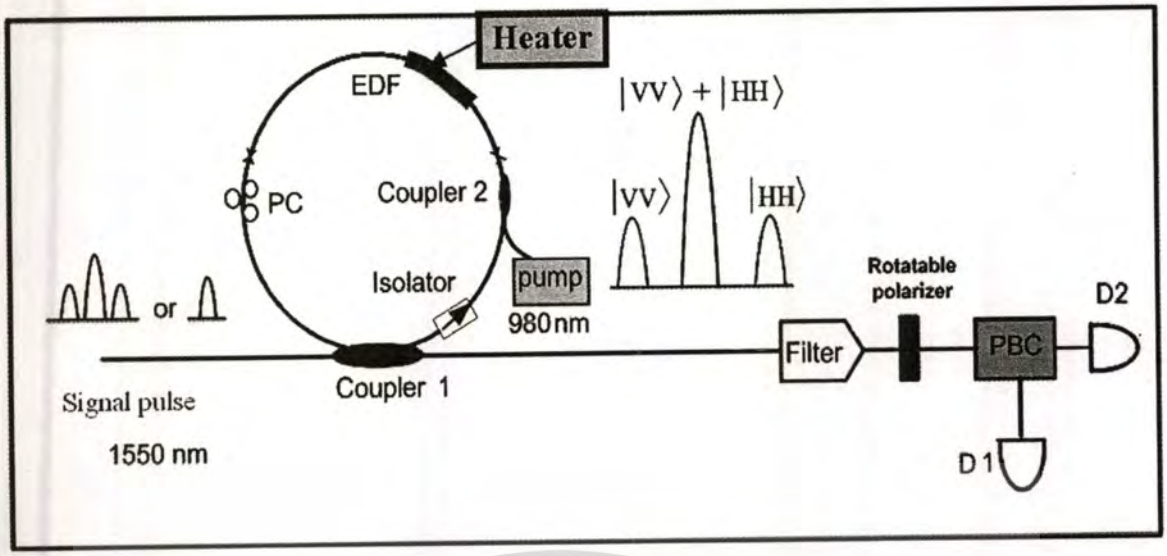

Fig. 6.7 A schematic diagram of an experimental setup fiber optic ring resonator incorporating an erbium-doped fiber.

The optical tunable filter with large tuning range is employed to obtain the entangled photon states at the required wavelengths, which means the selection of the detected signals (photons) could be desired. The Erbium-doped fiber can be designed to obtain precisely amplified signals, while the change in phase is controlled by using the polarization controller (PC). To investigate the entangled photons phase shift with temperature changes, a section of fiber ring resonator was laid in the temperature control environment. The polarization angles were rotated from 0 to 90 degree by tilting the PC. This caused the change of both entangled states and optical output intensity. To confirm the existence of entangled states, then each photon was input into a polarizer and orientation from 0 to 180 degree before launching into the PBC. The output photons were detected by the avalanche photodiodes.

6.3.2 Experiment Results

A plot of the optical output intensity of the system as is shown in Fig. 6.8, when a fiber section was laid in the control heating source unit. The entangled photon phase shifts compensation could be achieved after one the polarization control device was rotated. The polarization control devices were also taken, i.e. adjusted to obtain the optimum photon visibility. The relation between the entangled photon phase shifts and the rotation angles, i.e. walk-off length has not shown any significant assumption.

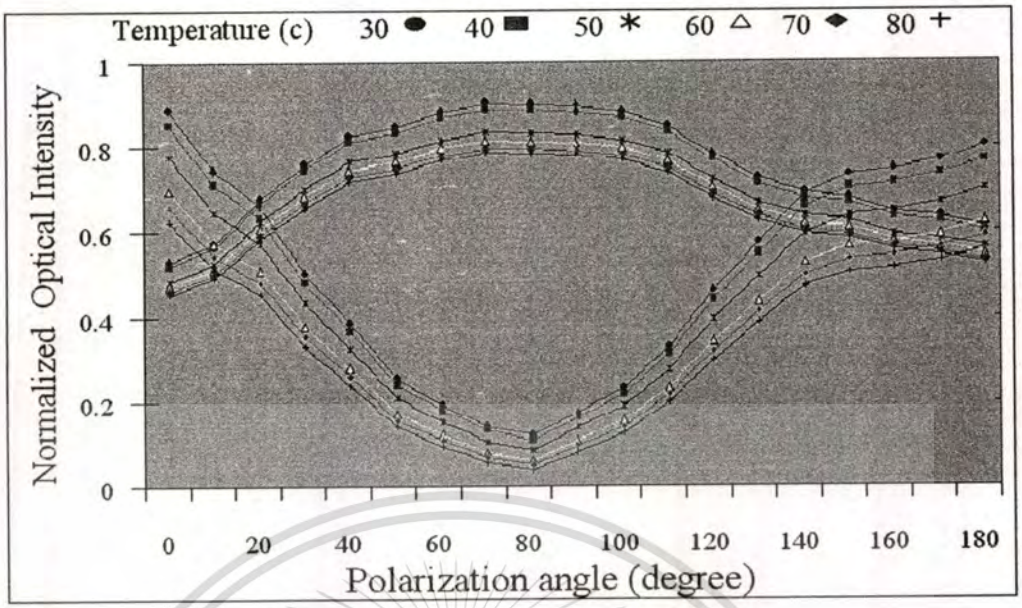

Fig. 6.8 Graph of the output intensity (Entangled Photon Visibility) and the polarization angle, when the fiber section is in the temperature control environment.

The relationship between the output intensity and temperature is also plotted as shown in Fig, 6.9. Where the loss of photon energy is presented and shown in term of the detected optical output (mV). Which is shown that the decreasing in the optical intensity when the decreasing temperature was from 30 to 80 $^{\circ}$C seen. This means that such a proposed system is still reliable to the change in temperature. The interesting result is that the entangled states walk-off compensations due to temperature changes could be achieved by using a pair of polarization control devices. Further, the recovery entangled two-photon state is possible with phase difference adjusting of the walk-off length, which is detected by the avalanche photo detectors D1 and D2. We also found that the noise floor of 0.3 (approximate) was occurred on the detectors. This was introduced before the operation of EDF which was lower than the amplified detected signals. However, this could be ignored comparing to the amplified signals, which means the system is still valid and reliable for the use of the entangled photon generation in some specific temperature ranges.

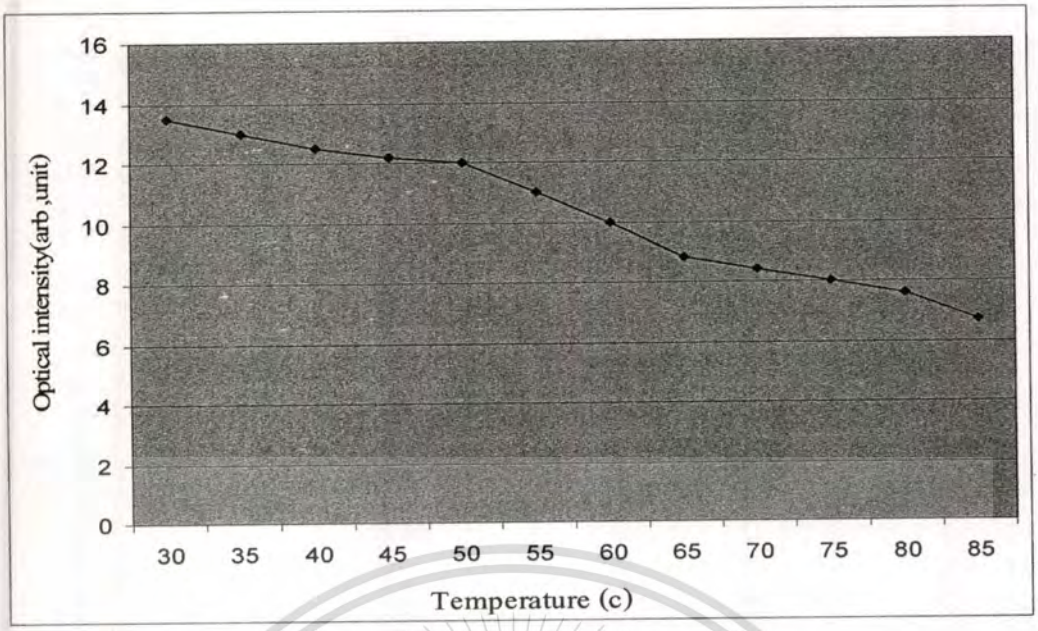

Fig. 6.9 Graph of the output intensity versus temperature.

The measurement of the change in temperature relating to the entangled states walk-off length or fiber birefringence is setup as shown in Fig.6.7. To obtain the optimum photon visibility of the entangled photons after walk-off compensation, then the measurement relationship between the polarization orientation phase shift and the temperature change is employed. The length of erbium-doped fiber is laid in the temperature control environment. The change in temperature introduced the change in phase (phase shift, $\Delta\phi$) of the entangled photons. The fiber birefringence, i.e. rotation angle is measured which can be compensated to obtain the optimum photon visibility. The measurement data is obtained by the detector D1 and D2, where the photon visibility is obtained. Result as shown in Fig.6.8 presents the optical intensity at the output of the polarization output. The control temperatures are 30, 40, 50, 60, 70, and 80 C^0 . Each case, photon was input into a polarizer and orientation, which was rotated from 0 to 180 degree before launching into the PBC. However, the off set value of the measurement data for measurement calibration is required before measurement operation. To recover the change in phase due to temperature change, the adjusting on the polarization angle of the polarization controller (PC) before the polarizing beam splitter is operated. Then the measured orientation angle is noted and plotted relatively to the change in fiber birefringence (Δn i.e. physical parameter). This means the entangled state walk-off is compensated.

CHAPTER 7

DISCUSSION AND CONCLUSIONS

7.1 Discussion

To begin this concept, we introduce the technique that can be used to create the entangled photons, the input pulses that the polarization states correspond to an optical switch (coupler) between the short and the long pulses, where the short and long pulses correspond to the pulses that traveling through short and long fiber lengths respectively. We assume those horizontally polarized pulses with a temporal separation of Δt . The coherence time of the consecutive pulses is larger than Δt . Then the following time-bin state can be writing in Eq. (7.1).

$$|\Phi\rangle_P = |1,H\rangle_s|1,H\rangle_i + |2,H\rangle_s|2,H\rangle_i \tag{7.1}$$

In the expression of $|k,H\rangle$, k is the number of time slots ($k=1,2$), the state of polarizations are denoted by horizontal (H) or vertical (V), and the subscripts imply the state of the signal (s) or the idler (i). In Eq. (7.1), for simplicity we have omitted an amplitude term that is common to all product states, which similar in subsequent equations in this paper. The two-photon states with H polarization as shown in Eq. (7.1) are the input into the orthogonal polarization-delay circuit (fiber ring resonator).

$$\begin{aligned}|\Phi\rangle = {} & |1,H\rangle_s|1,H\rangle_i + \exp(i\phi_i)|1,H\rangle_s|2,V\rangle_i + \exp(i\phi_s)|2,V\rangle_s|1,H\rangle_i \\ & + \exp[i(\phi_s+\phi_i)]|2,V\rangle_s|2,V\rangle_i + |2,H\rangle_s|2,H\rangle_i + \exp(i\phi_i)|2,H\rangle_s|3,V\rangle_i \\ & + \exp(i\phi_s)|3,V\rangle_s|2,H\rangle_i + \exp[i(\phi_s+\phi_i)]|3,V\rangle_s|3,V\rangle_i\end{aligned} \tag{7.2}$$

By the coincidence counts in the second time slot, we can extract the fourth and fifth terms. As a result, we can obtain the following polarization entangled state as

$$|\Phi\rangle = |2,H\rangle_s|2,H\rangle_i + \exp[i(\phi_s+\phi_i)]|2,V\rangle_s|2,V\rangle_i \tag{7.3}$$

In case of the system using weak light input (i.e. without pumping part and component), the fiber acts as a nonlinear medium because of the Kerr effects and four-wave mixing of light in a fiber

ring resonator. The weak light source in this case is the commercial diode laser, which the output power is ranged from 3-5 mW. The superposition of the delayed pulse trains within the fiber ring resonator can introduce the Kerr effect and FWM at the resonance power.

When a polarized pulse or polarization entangled photon enters into a fiber ring resonator incorporating an erbium-doped fiber (EDF), the nonlinear effect i.e. Kerr type occurs which is induced the entangled states in Eq.7.3. An optical amplifier is operated by EDF via a coupler 1, where the output is then re-circulated within the ring resonator. The resonator re-circulating power is extracted from the coupler 1, which means there is part of the optical power leaving the fiber ring resonator. Where γ and κ are the fractional intensity loss and intensity coupling coefficient of the coupler 1. Fiber attenuation and the fiber ring length are represented as α and L, respectively. The fractional over-all loss of optical components in the ring is η. This includes the power which is extracted by a coupler 2. Full resonance, in particular, is obtained when the round-trip intensity loss through the ring is just compensated for by the fractional intensity coupling at the coupler 1. Thus, full resonance of an optical amplifier with an intensity gain (G) can be written as

$$G = \frac{e^{2\alpha L}}{(1-\gamma)(1-\eta)(1-\kappa)} \tag{7.4}$$

When H and V are the states of polarization [horizontal (H) or vertical (V)], and the subscript identifies whether the states is the signal (s) or the idler (i) state. In Eq. (7.1), for simplicity we have omitted an amplitude term that is common to all product states. As a result, we can obtain the following polarization entangled states. In general, the weak entangled photon states can also be recovered after circulating in the amplified fiber optic medium and the photon states can be re-generated by adjusting the polarization controller (PC) of the amplified photons, where the regenerated entangled states can be achieved.

Initially, the optimum entangled photon visibility is formed by using two polarized control devices, which one is the PC, the other is the rotatable polarizer. The change in transversal walk-off from the optimum point can be recovered by adjusting the rotatable polarizer. The transversal walk-off produces a shift between the ordinary and extraordinary while the longitudinal walk-off introduces a time delay between horizontally and vertically polarized photons. Finally, the change in fiber birefringence where a transversal walk-off (the extraordinary

beam) and the longitudinal walk-off between the ordinary and extraordinary beam is occurred. The amount of the walk-off depends on the location where the photon-pairs are created within the fiber. This position is completely random due to the coherent nature of light in fiber optic. To compensate the longitudinal timing-walk-off effect, a polarization controller is recommended to ensure that the polarization rotation is the same on both photons from the entangled pair. Additionally the compensator fiber is used to change the relative phase ϕ of the states of the polarized light. In this case the compensation is made by the polarization rotation angle of the rotatable polarizer. Because of the change in birefringence, the tilting of the compensator allows to apply a phase shift to the entangled states of the two photons, which are given by Eq. (7.5).

$$|\psi\rangle_{12} = \frac{1}{\sqrt{2}}\left(|H\rangle_1 \otimes |V\rangle_2 + e^{i\phi}|V\rangle_1 \otimes |H\rangle_2\right) \tag{7.5}$$

In applications, the walk-off entangled state parameters involving in the measurement are related to the changes in the applied physical parameters such as force, stress, strain, heat, and pressure etc and the fiber optic properties. However, the interested parameters in this proposed systems are concerned the fiber optic birefringence parameters, which can be given by

$$\Delta\phi = \frac{2\pi (n_x - n_y) L_w}{\lambda} \tag{7.6}$$

Where $\Delta n = (n_x - n_y)$ is the fiber optic birefringence, L_w is the entangled states walk-off length, and λ is the light source wavelength. In principle, the measurement of the change in applied physical parameter relating to the entangled states walk-off length or fiber birefringence is proposed. When the applied physical parameter is employed to the erbium-doped fiber within the temperature control environment, the entangled photons walk-off states is induced, where the change in temperature can be induced the change in phase shift ($\Delta\phi$)]. To obtain the optimal visibility of the entangled photons after walk-off states. The photon states can also be recovered after circulating in the amplified fiber optic medium by adjusting the polarization controller (PC) or change a temperature of the amplified photons, where the regenerated entangled states can be achieved. The measurement data is obtained by the detector D1 and D2.

7.2 Conclusion

We have demonstrated the use of our scheme which is consisted of a fiber ring resonator incorporating the EDF, where the low optical power entangled states recovery is achieved. The results obtained have shown that the entangled states with the lower input can be regeneration with higher amplitude by pumping EDF and tilting PC, respectively. Further, the rotatable polarizer was rotated to obtain the optimum entangled photon visibility. The purposed system can be used to recover the low polarized input light pulse, the entangled photons and walk-off compensation, while the entangled states can be recovered and suitable for long distance quantum communication link. Where the repeated signal in the transmission line is plausible, which means the use of a quantum repeater could be realized.

The system generation the dynamic simulation of light traveling in nonlinear fiber, where the low optical power entangled states recovery. The optical nonlinear phenomena including the bistability and the Ikeda instability such as the bifurcation and chaos are investigated. This system can be used to recover both low polarized input light pulse or polarization entangled states.

We have proposed and successfully demonstrated a stable and broad bandwidth multi wavelength EDFL with potential applications in DWDM systems. Nonlinear optical loop mirrors which induces intensity-dependent loss in a laser cavity and functions as an amplitude equalizer was employed to obtain stable multi wavelength oscillations in EDFL at room temperature. Multi wavelengths lasing operation with uniform power distribution has been achieved.

The test of thermal effects on the walk-off entangled states is discussed, which is ignorable after the compensation. The nonlinear response time for the 1550 nm light signal is very fast, because 1550 nm is a resonant wavelength i.e. center wavelength of the amplified medium. However, the detected output still can be performed the entangled photon visibility and valid. A result of the change in entangled photon states due to temperature changes have shown the interesting result, where the optimum photon visibility can be achieved by adjusting a pair of the polarization control devices. Which means the entangled photon states walk-off due to the change in temperature can be compensated and achieved by using a pair of the polarization control devices.

The main advantage of the fiber-based sources entangled photons is the good compatibility and reliability with the transmission fiber system. This system can also be used to recover both low polarized input light pulse or polarization entangled states, while the entangled

states can be recovered and suitable for long distance quantum communication link. However, the fiber ring radius is a long fiber length. Therefore, in practices, we still require the shorter amplified fiber to use in the practical system. This will be the interesting subject of the research project in the future.

REFERENCES

[1] T. S. Manderbach, H. Weier, M. Furst, R. Ursin, F. Tiefenbacher, T. Scheidl, J. Perdigues, Z. Sodnik, C. Kurtsiefer, A. Zeilinger and H. Weinfurter, "Experimental Demonstration of Free-Space Decoy-State Quantum Key Distribution over 144 km," Phys. Rev. Lett. 98, 010504 (2007).

[2] M. Pfennigbauer, M. Aspelmeyer, W. Leeb, G. Baister, T. Dreischer, T. Jennewein, G. Neckamm, J. Perdigues, H. Weinfurter, and A. Zeilinger, "Satellite-based quantum communication terminal employing technology," J. Opt. Netw. 4, 549-560 (2005).

[3] S. Suchat, W. Khannam and P.P. Yupapin, "Quantum Key Distribution via an Optical Wireless Communication Link for Telephone Networks," Opt. Eng. (2007). (Excepted)

[4] P. van Loock, T. D. Ladd, K. Sanaka, F. Yamaguchi, Kae Nemoto, W. J. Munro and Y. Yamamoto, "Hybrid Quantum Repeater Using Bright Coherent Light," eprint: quant-ph/0510202 (2006).

[5] P.P. Yupapin and S. Suchat, "Entangled Photon Generation using Fiber Optic Mach-Zehnder Interferometer Incorporating the Nonlinear Effect in a Fiber Ring Resonator," J. Nanophotonics (JNP), 1, 013504 (2007).

[6] P.P. Yupapin et al., "Coupler-loss and Coupling-coefficient Dependent of Bistability and Stability in a Fiber Ring Resonator : Nonlinear Behaviors", World Scientific : Journal of Nonlinear Optical Physics and Material Science (JNOPM), Vol.16, No.1, March, 2007

[7] P.P. Yupapin et al., "An Investigation of the Entangled Photon Walk-off Compensation Generated by a Fiber Ring Resonator" , International Journal of Light and Electron Optics, 2008.

[8] P.G. Kwiat, K. Mattle, H.Weinfurter, A. Zeilinger, A.V. Sergienko, and Y. Shih, "New high-intensity source of polarization-entangled photon pairs", Phys. Rev. Lett.75, (1995).

[9] J.D.Franson, "Bell inequality forposition and time", Phys. Rev. Lett.62, 2205-2208 (1989).

[10] X. Li, P. L. Voss, J. E. Sharping, and P. Kumar, Phys. Rev. Lett. 94(2005)053601.

[11] D. Bouwmeester, A.Ekert, and A. Zeilinger , "The Physics of Quantum Information", Springer, Berlin, (2000).

[12] V. Giovannetti, S. Lloyd, L. Maccone, "Quantum Metrology", quant-ph/0509179 v1, 2005.

[13] H. Takesue, K. Inoue, O. Tadanaga, Y. Nishida, and M. Asobe, Opt. Lett. 30(2005)293.

[14] D. I. Fivel, "The Prime Factorization Property of Entangled Quantum States", High Energy Physics– Theory /9409150v1(1994).

[15] E. A. J. Marcatili. "Dielectric Rectangular Waveguide and Directional Coupler for Integrated Optics." Bell. Syst. Tech. J., vol. 48, September 1969. pp. 2071-2101.

[16] C. K. Madsen and J. H. Zhao. "A General Planar Waveguide Autoregressive Optical Filter." IEEE J. Lightwave Tech., vol. 14, no. 3, March 1996. pp. 437-447

[17] S. C. Hagness et al.. "FDTD Microcavity Simulations: Design and Experimental Realization of Waveguide-Coupled Single-Mode Ring and Whispering-Gallery-Mode Disk Resonators," IEEE J. Lightwave Tech., vol. 15, no. 11, November 1997.

[18] D. Rafizadeh et al.. "Waveguide-coupled AlGaAs/GaAs microcavity ring and disk resonators with high finesse and 21.6 nm free spectral range." Opt. Lett., vol. 22, no. 16, August 1997. pp. 1244-1246

[19] B. E. Little et al.. "Ultra-Compact Si-SiO_2 Microring resonator Optical Channel Dropping Filters." IEEE Photon. Techn. Lett., vol. 10, no. 4, April 1998. pp. 549-551

[20] D. J. W. Klunder et al., "Vertically and laterally waveguide-coupled cylindrical microresonators in Si_3N_4 on SiO_2 technology." Appl. Phys. B 73., November 2001. pp. 603-608

[21] A.Einstein, B. Podolsky, and N.Rosen, "Can quantum-mechanical description of physical reality be considered complete", Phys. Rev. 47, 777-780 (1935).

[22] J.S.Bell, "On the Einstein-Podolsky-Rosen paradox", Physics 1, 195-200 (1964).

[23] J.F.Clauser, M.A. Horne, A.Shimony, and R.A. Holt, "Proposed experiment to test local hidden-variable theories", Phys. Rev. Lett. 23, 880-884 (1969).

[24] J.F.Clauser and A. Shimony, "Bell's theorem: experimental tests and implications",Rep. Progr. Phys. 41, 1881-1927 (1978).

[25] A.Aspect, P. Grangier, and G. Roger, "Experimental tests of realistic local theories via Bell's theorem", Phys. Rev. Lett. 47, 460-463 (1981).

[26] C. O.Alley and Y. H. Shih, "Proceedings of the Second International Symposium on Foundations of Quantum Mechanics in the Light of New Technology", Tokyo, 1986 (Physical Society of Japan,Tokyo, 1987).

[27] A. Ekert, "Quantum cryptography based on Bells theorem", Phys. Rev. Lett.67, 661-663 (1991).

[28] N. Gisin,G. Ribordy, W. Tittel,and H. Zbinden,"Quantum cryptography", Rev. Mod. Phys. 74, 145-190 (2002).

[29] C. Bennett, G. Brassard, C. Crepeau, R. Jozsa, A. Peres, and W.K. Wootters, "Teleporting an unknown quantum state via dual classical and Einstein-Podolsky-Rosen channels", Phys. Rev. Lett.70, 1895-1899 (1993).

[30] D. Bouwmeester, J.W.Pan, K.Mattle, M. Eibl,H. Weinfurter, and A. Zeilinger, "Experimental quantum teleportation", Nature 390, 575-579 (1997).

[31] M.A. Nielsen and I.L.Chuang, "Quantum computation and quantum information", Cambridge University Press,Cambridge, 2000.

[32] R.A. Bertlmann and A. Zeilinger, eds., "Bells theorem: the naive view of an experimentalist" Springer-Verlag, Berlin, 2002.

[33] D.N. Klyshko, "Photons and Nonlinear Optics", Gordon and Breach Science, New York, 1988.

[34] D.C. Burnham and D.L. Weinberg, "Observation of simultaneity in parametric production of optical photon pairs", Phys. Rev. Lett.25, 84-87 (1970).

[35] P.G. Kwiat, E.Waks, A.G. White,I. Appelbaum, and P.H. Eberhard, "Ultra bright source of polarization-entangled photons", Phys. Rev. A 60, R773-R776 (1999).

[36] P.G. Kwiat, "Hyper-entangled states", J.Mod. Opt. 44, 2173-2184 (1997).

[37] M. Atature, G. Di Giuseppe, M.D. Shaw, A.V. Sergienko, B.E.A. Saleh, and M.C. Teich, "Multiparameter entanglement in quantum interferometry", Phys. Rev. A 66, (2002).

[38] T.B. Pittman, D.V. Strekalov, D.N. Klyshko, M.H. Rubin, A.V. Sergienko, and Y.H. Shih, "Two-photon geometric optics",Phys. Rev. A 53, 2804-2815 (1996).

[39] C.H. Monken, P.H. Souto Ribeiro, and S. Padua, "Transfer of angular spectrum and image formation in spontaneous parametric down-conversion", Phys. Rev. A 57, (1998).

APPENDIX

List of Publication

1. W. Khunnam and P.P. Yupapin, **An Investigation of the Entangled Photon Walk-off Compensation Generated by a Fiber Ring Resonator,** International Journal of Light and Electron Optics, 2008.DOI : 10.1016/j.ijleo.2008.02.025 (Impact Factor 2006:0.589)

2. S. Suchat, W. Khunnam and P. P. Yupapin, **The Entangled Photon States Recovery using a Fiber Ring Resonator Incorporating an Erbium-doped Fiber Amplifier,** Optical Engineering, Vol. 47(6), 2008, pp. 100502-1-5.(Impact Factor:2007:1.24) Has been selected for **"Covering a focused area of Frontier Research"** in the July 2008 issue of Virtual Journal of Quantum Information. The Virtual Journal, which is published by the American Physical Society **(APS)** and the American Institute of Physics **(API)**.

3. W.Khunnam, S. Suchat and P.P.Yupapin , **Entangled Photons Generation and Regeneration using a Nonlinear Micro Ring Resonator,** JNOPM, Special Issue Volume, September, 2008. (Impact Factor 2006:0.496)

4. W. Khunnam and P.P.Yupapin, **The Entangled Photons Regeneration and Characterization in Nonlinear Fiber Ring Resonator,** SPIE-Volume 6793, 2008. DOI:10.1117/12.799529

5. S. Suchat, W. Khannam and P.P. Yupapin, **Quantum Key Distribution via an Optical Wireless Communication Link for Telephone Nework,** SPIE : Optical Engineering Letters, Vol.46(10), 2007, pp.100502.(Impact Factor 2006:0.897)

6. P.P. Yupapin, W. Khunnam and S. Suchat, **The Entangled Photons Generation System Using Weak Light in Fiber Optic and Timing-walk off Compensation,** International Journal of Quantum Information,Vol.5(6),2007,pp.805-814.
DOI :10.1142/S0219749907003249 (Impact Factor:0.681)

BIOGRAPHY

NAME	**MR. Wanchai Khunnam**
DATE OF BIRTH	**25 DECEMBER 1976**
PLACE OF BIRTH	**Mahasarakham, Thailand.**
	E-mail: Chai_kh@hotmail.com

QUALIFICATIONS

EDUCATION

- Bachelors of Science(Physics) Naresuan University, Pitsanulok ,Thailand in 1998.
- Masters of Science (Applied physic) at Advanced Research Center for Photonic Laboratory, King Mongkut's Institute of Technology Ladkrabang, Bangkok, Thailand in 2002.

EXPERIENCE

- Lecturer at Department of Physics Faculty of Science Naresuan University (NU), Pitsanulok, Thailand. (1999-Present)

SKILLED WORKS

- Fiber Optics Communications
- Electric & Electronic
- Telecommunications & Computer Network
- Fiber Optics Sensor
- Quantum Information.